



A new candidate for optoelectronic device applications: CoTiX (X: P, As, Sb) half-heusler compounds

İlknur Kars Durukan^{a,*}, Yasemin Oztekin Ciftci^a, Hatice Tekin^b

^a Department of Physics, Gazi University, Teknikokullar, 06500, Ankara, Turkey

^b Department of Condensed Matter Physics, Institute of Science, Gazi University, Teknik Okullar, 06500, Ankara, Turkey

ARTICLE INFO

Keywords:

DFT
Half-heusler
Elastic
Ductile
Optoelectronic
Thermodynamic

ABSTRACT

Some theoretical calculations of CoTiX(X:P, As, Sb) Half-Heusler(HH) compounds in MgAgAs-type structure have been analyzed using density functional theory (DFT). These Half-Heusler compounds are stable mechanically, and CoTiAs are entirely isotropic, whereas CoTiP and CoTiSb are anisotropic. Mechanical properties indicate that they have a ductile nature in all three compounds. In addition, elastic properties are presented in three dimensions (3D) for detailed analysis of Young's modulus, linear compressibility, shear modulus, and Poisson's ratio. Electronically, the investigated compounds are semiconductors with an indirect bandgap. The calculated positive phonon vibration frequencies of these Half-Heusler compounds show their dynamic stability in the cubic MgAgAs phase. Optical parameters such as dielectric function, reflectivity, absorption coefficient, refractive index, loss function, and absorption coefficient are given in IR, visible, and ultraviolet regions according to considerable photon energies. Finally, the effects of pressure and temperature on thermodynamic properties are discussed in detail.

1. Introduction

Recently, the breadth of work in materials science has been concerned with developing new materials [1–7]. As a family of intermetallic compounds with more than 1500 compounds that can be formed, Heusler compounds offer a suitable study area for new material design due to its wide composition range and adjustable material properties. Most Heusler compounds are magnetic intermetallic, and their crystal structure is face-centered cubic. Heusler compounds consist of two classes, 1:1:1 (half Heusler) or 2:1:1 (full Heusler), formed by different stoichiometries of the three elements. It can be defined by the prototypes L21 and C1b with space groups Fm3m (No = 225) and F43 m (No = 216) for full and half Heusler, respectively. X and Y are transition metals, and Z is an sp element. Half-Heusler compounds with 8 or 18 valence electrons usually denote band gaps that depend on s, p, and d electron shells [8]. Half-Heusler materials with 8 valence electrons are very similar to the basic physical properties of known semiconductors such as GaAs and Si [9–11]. Half-Heusler compounds with 8 valence electrons increase the band gap when the difference between the electronegativity of the X and Y atoms in their compounds increases. While the band gap of Half-Heusler compounds with 18 valence electrons can be adjusted to a

width of 0–1 eV, this value can reach up to 4 eV for all half-Heusler compounds [12]. Half-Heusler compounds with 18 valence electrons are suitable for thermoelectric materials due to their lower band gaps [13–17].

Half-Heusler compounds have areas of use for different applications. Half-Heusler compounds have attracted attention in optoelectronic applications such as thin-film solar cells and laser diodes, in thermoelectric applications due to their band gaps, in spintronic applications with their Fermi-level spin polarization and high Curie temperatures [9,18–25]. Also, Half-metals are considered ideal electrode materials for magnetic tunnel junctions and giant magneto-resistor devices for injecting spin-polarized currents into semiconductors [26–28].

The progress and enhancement of optoelectronic devices heavily rely on the presence of appropriate semiconductor materials. Recently, there has been a noticeable inclination towards utilizing multinary compounds, which offer a broader spectrum of electrical, optical, and chemical properties. This shift is driven by the need for materials tailored to meet specific requirements in optoelectronic devices. The Half-Heusler semiconductors constitute a noteworthy subset within the HH category. These materials, devoid of magnetic properties, showcase a variable gap from 0 eV to 4 eV [29–33]. Initially synthesized and

* Corresponding author.

E-mail address: ilknurdurukan@gazi.edu.tr (İ. Kars Durukan).

examined by Nowotny-Jusa [34,35], researchers widely investigate these HH semiconductors due to their relevance in optoelectronic materials.

Additionally, their capacity for alloying introduces the potential to minimize thermal conductivity [36–38]. Kieven et al. presented the results of their first-principle calculations, aiming to identify the potential of half-Heusler compounds for utilization in optoelectronic devices. The authors utilized two criteria to select suitable half-Heuslers for a buffer layer material: a band gap greater than 2 eV to mitigate absorption losses and a lattice parameter of approximately 5.9 Å to align with the crystal structure of the absorber material [19]. During their research, the authors identified seven materials that satisfy these criteria.

Ti, Zr, Hf; Co, Rh, Ir; and P, As, Sb, Bi atoms belong to groups IV-IX-V of the periodic table, respectively, and compounds consisting of these atoms have interesting physical properties [39,40]. These ternary Half-Heusler compounds have been the subject of many theoretical and experimental studies regarding thermoelectric, optoelectronic, and electronic device applications [12,41–56]. Sekimoto et al. successfully experimentally synthesized (Ti, Zr, Hf)CoSb samples using the arc melting technique and determined their thermoelectric properties [49]. With this work, they discovered new materials that have the potential to be a thermoelectric material group. Zhao et al. experimentally synthesized the polycrystalline of Pd-doped ZrCo_{1-x}Pd_xBi ($x = 0, 0.03, 0.06, 0.09$) Half-Heusler samples using rapid hot pressing sintering and arc melting techniques. They determined that the Seebeck coefficient and electrical conductivity increased due to the displacement of Pd with the Co atom [50]. It was emphasized that it provides a fundamental basis for obtaining efficient and cost-effective HH compositions. Chauhan et al. experimentally have synthesized (Ti, Zr)Co_{1+x}Bi_{1-y}S_y ($x = 0, 0.03, 0.05, 0.07; y = 0, 0.20$) by vacuum arc melting under a protective atmosphere of high purity Ar. With the study, it was found that for optimized p-type ZrCo_{1.03}Sb_{0.8}Sn_{0.2} HH nanocomposites, a maximum ZT of ~0.7 was obtained at 873 K, which is among the highest values obtained in p-type HH alloys [42]. Xia et al. experimentally produced ZrCoSb and HfCoSb compounds using arc melting. These compounds showed semi-metal properties at room temperature and had low Seebeck coefficients, and they also found that their thermoelectric properties could not be optimized [43]. As for the theoretical studies, the phonon and thermoelectric properties of the HfRhSb HH compound were analyzed by Kaur et al. using the Quantum Espresso package. This compound was determined to have an indirect band gap of 1.21 eV⁴¹. The structural, electronic, magnetic, and lattice dynamics of XCoBi (X: Ti, Zr, Hf) HH compound were calculated for three different phases by Surucu et al. the DFT method. It was determined that the most stable phase was the γ phase [44]. Gautier et al. analyzed over 400 HH compounds using the Heyd-Scuseria-Ernzerhof (HSE) hybrid functional [51]. A recent study analyzed the structural and electronic properties of ZrCoBi and ZrRhBi compounds. This study concluded that ZrCoBi has a higher Seebeck coefficient and lower electrical conductivity than ZrRhBi [53].

Many studies on co-based HH compounds with ternary structures are available in the literature. However, no study on CoTiX (X:P, As, Sb) HH compounds has been found in the literature. In our previous study, structural, vibrational, and thermodynamic properties of CoTiSb compound were analyzed by DFT [57–60] method. In our study, the structural, mechanical, anisotropy, vibrational, optical, and thermodynamic properties of the mentioned compounds were evaluated in detail. The theoretical presentation of the versatile analysis of compounds is essential in terms of being a resource for experimental researchers dealing with materials science.

2. Computational method

All calculations based on geometric optimization were calculated using the DFT method [61–63] using the Vienna ab initio simulation package program (VASP) [62,64,65]. Perdew–Burke–Ernzerhof

parameterization (PBE) was used for exchange–correlation function using the generalized gradient approach (GGA) [66]. In the geometric optimizations of this study, the energy-convergence criteria were set at 10^{-8} eV/atom. The energy cut-off value related to plane waves was established at 700 eV, and a $15 \times 15 \times 15$ grid mesh of Monkhorst and Pack [67] k-points was employed, sampling along the high symmetry directions of the Brillouin zone for CoTiX (X:P, As, Sb) HH compounds. The geometry optimization utilized the MethFessel-Paxton smearing approach, and the tetrahedron method with Blochl corrections was applied for total energy calculations. The valence-electron configurations for the Co, Ti, P, As, and Sb are [Ar] 3 d⁷ 4s², [Ar] 3 d² 4s², [Ne] 3s² 3p³, [Ar] 4s² 4p³ and [Kr] 5s² 5p³, respectively. Mechanical properties were calculated using the stress-strain method [68] with the help of IBRION = 6 commands implemented in VASP 5.4. The representation of the three-dimensional anisotropy properties of the mechanical properties was done with the VELAS code [69]. Phonons of CoTiX were determined using a supercell approach to elucidate vibrational characteristics. Real-space force constants were analyzed by implementing density functional perturbation theory in the VASP code. The supercell approach determined the analysis of vibration properties. The PHONOPY code is used to calculate phonon frequencies [70]. The dependence of the thermodynamic properties of CoTiX (X:P, As, Sb) half heusler compounds on pressure and temperature was tested using the semi-harmonic Debye model [40,47,71,72] approach via the GIBBS code.

3. Results and discussion

3.1. Structural properties

The diagram of the total energy changes versus the volume change of the unit cell gives information about the structural stability [73]. Fig. 1a displays the optimized energy as a function of volume (E-V) for CoTiX (X: P, As, Sb) HH compounds, calculated based on Murnaghan Equation [74]. From Fig. 1a, Energetically, CoTiP is the most stable between CoTiX(X: P, As, Sb). The energy-volume curve in Fig. 1a illustrates a correlation between cell volume and energy. According to the research results, there is a decreasing trend in cell energy as the volume expands, reaching a minimum value identified as the ground state energy. Beyond this point, the energy rises as the cell volume increases, indicating a shift toward system instability.

The detailed information of Fig. 1a for CoTiX (X: P, As, Sb) HH compounds is presented in Table 1. CoTiX (X: P, As, Sb) HH compounds consist in a face-centered-cubic (fcc), MgAgAs-type structure with space group F43 m (No. 216) illustrated in Fig. 1b and created in VESTA 3D-program. The unit cell contains three atoms, with Co, Ti, and X (P, As, Sb) atoms located at the (0.25, 0.25, 0.25), (0.5, 0.5, 0.5), and (0.0, 0.0, 0.0), Wyckoff positions [75], respectively.

The structural parameters, lattice parameters (a_0), bulk modulus (B), the first-order pressure derivative of bulk modulus (B'), and volume (V) of CoTiX (X: P, As, Sb) HH compounds are presented in Table 1. The lattice constant values of the compounds are compatible with the experimental and theoretical studies in the literature [76]. For CoTiSb, our calculated lattice constants are 0.0067% higher than the experimental value 5.883 Å. Table 1 shows that while the value of the lattice constant increases, the value of the bulk modulus decreases from P to Sb elements. P, As, and Sb are elements with similar chemical properties in group 5 A in the periodic table. The atomic radius of P, As, and Sb is 1 Å, 1.15 Å, and 1.45 Å, respectively. In this case, the atomic radius is directly related to the lattice constants of the compounds [77]. Bulk modulus is one of the necessary parameters for the evaluation of the hardness of the material. The decrease of the bulk modulus indicates that the hardness of the compounds changed as CoTiP > CoTiAs > CoTiSb. Thus, compounds with larger lattice constants are easier to compress than those with smaller ones. Pressure derivatives of Bulk modulus for the CoTiX compounds increase from CoTiP to CoTiSb,

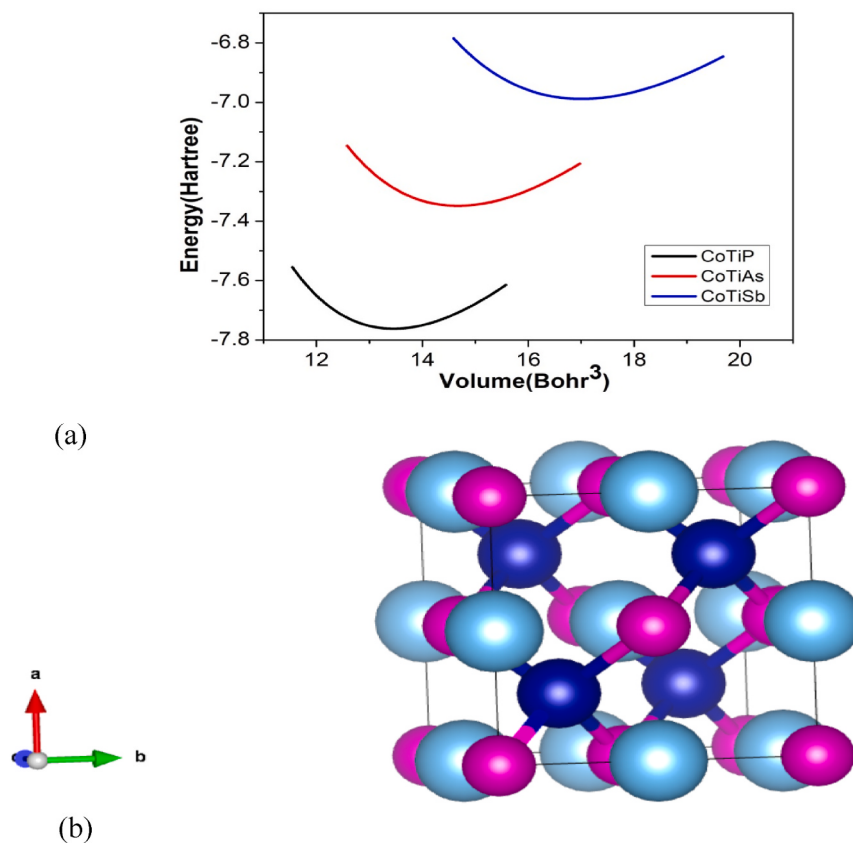


Fig. 1. a) The E-V diagrams of the CoTiX (X: P, As, Sb) HH compounds, b) Unit cell of CoTiX (X = P, As, Sb) compounds showing the three occupied sub-lattices. Dark blue circles Co atoms, blue circles Ti atoms, pink circles X atoms.

Table 1
Structural parameters of CoTiX (X: P, As, Sb) HH compounds.

Material	a(Å)	B(GPa)	B'	V(Å³)
CoTiP	5.445 5.43 ⁷⁶ , 5.43 ⁷⁶ , 5.4372 [76]	184.6	4.52	40.4
CoTiAs	5.604 5.61 ⁷⁶	164.3	4.54	44
CoTiSb	5.887 5.88 ⁷⁶ 5.883 [79] 5.886 [80]	142.8 122.517 [80]	4.6 5.848 [80]	51

indicating that by applied pressure, CoTiSb is more affected than the other two compounds for Bulk modulus. As a result, we can say heavier compounds are more compressible than lighter ones. The theoretical calculations provide values that are slightly elevated compared to the experimental results, a phenomenon commonly associated with the tendency of DFT GGA to overestimate lattice constants. Nevertheless, the consistency between the two data underscores the dependability of the computational methodology utilized in this study.

Slater-Pauling behavior of Heusler alloys in terms of magnetic properties exhibits. For Half-Heusler alloys, since the 9 spins down band are filled, the total magnetic moment is expressed with $Mt = (Zt - 18) \mu B$ rule, where Zt is the sum of the valence electrons in the alloy or the number of spin-up and spin-down electrons ($Zt = N \uparrow + N \downarrow$). For CoTiX (X = P, Sb, As) due to $Zt = 18$ values, the total magnetic moment is zero μB , indicating nonmagnetic behavior [78]. As a result, when we added spin-polarized calculations, we did not find any magnetic properties.

3.2. Elastic properties

Knowledge of a material's mechanical properties is an indispensable requirement for various professionals, ranging from materials scientists and engineers involved in composites for aeronautics and automotive industries [81,82] to those focused on pharmaceutical crystals [83–85] and biomaterials [86–88]. The mechanical attributes of a material offer valuable insights into its durability, resistance to damage, and potential applications. We are witnessing the widespread adoption of mechanically intricate materials such as shape-memory alloys [89], flexible electronics [90], ferroelastics [91–93], and other innovative materials. Recent extensions of Pugh's mechanical analysis have proven instrumental in deriving hardness descriptors, aiding the exploration of new materials for hard coating applications [94]. This analytical approach has also guided researchers in pursuing inorganic compounds surpassing diamonds in hardness. Elastic tensors serve as practical tools for screening materials with specific thermal properties, enabling estimating trends in heat capacities and thermal conductivity [95,96]. Furthermore, elastic properties find extensive applications in geophysics, where acoustic velocities assist in interpreting seismic data [97,98].

The response of materials used in engineering applications under stress and strain is significant. Elastic constants of materials are the key to mechanical properties. Therefore, any information such as hardness, ductility, chemical bond structure, plasticity, anisotropy, sound speeds, Debye temperature, melting temperature, etc. is accessed with this elastic constants [77].

In the computation of elastic properties, the preservation of crystal symmetry is crucial; otherwise, stiffness and compliance tensors may be inaccurately determined. To assess the mechanical stability of a crystal, the Born–Huang elastic stability criteria specific to the crystal system under consideration can be applied. The cubic system has three

independent elastic constants, C_{11} , C_{12} , and C_{44} , calculated using suitable lattice distortions. Mechanical stability of CoTiX (X:P, As, Sb) HH compound checked with five criteria ($C_{11} > 0$, $C_{44} > 0$, $C_{11} > C_{12}$, $C_{11} + 2C_{12} > 0$, $C_{12} < B < C_{11}$) for cubic crystals [99]. If any of these criteria are not met, it results in negative eigenvalues for the elastic tensor, indicating mechanical instability in the crystal. The piezoelectric response is inversely related to the elastic stiffness, so overestimating the flexibility of a material may lead to an overestimation of the electro-mechanical coupling. Consequently, conducting thorough mechanical testing on piezoelectric materials is highly advisable. Properties such as fracture limit and hardness are decisive in determining the specific applications and environments where the material can be effectively employed. Table 2 shows that CoTiX (X:P, As, Sb) HH compounds are mechanically stable. The calculated elastic constant values for CoTiP, which is more stable energetically, are higher than those of others, as seen in Table 2. Also, for the three investigated compounds, C_{11} values are bigger than those of C_{12} and C_{44} , showing that these compounds are more stable and harder to compress along X-axes.

The mechanical properties such as bulk modulus B (GPa), Shear modulus G (GPa), Young's modulus E (GPa), hardness Hv (GPa), plasticity measurement (B/C_{44}), B/G ratio, $C_{11}-C_{44}$ Cauchy pressure (GPa), Poisson's ratio (ν), Zener anisotropy factor (A), Debye temperature (θ_D , K), Melting temperature($T_m \pm 300$, K), and sound velocities(V_l (m/s), V_t (m/s) and V_m (m/s)), which are obtained from C_{ij} , can be given as Eq. (1)–(10) [100–107].

$$B = \frac{1}{3}(C_{11} + 2C_{12}) \quad [1]$$

$$G = \frac{1}{5}(C_{11} - C_{12} + 3C_{44}) \quad [2]$$

$$E = \frac{9BG}{3B + G} \quad [3]$$

$$\nu = \frac{3B - 2G}{2(3B + G)} \quad [4]$$

$$H_v = 2 \left(\left(\frac{G}{B} \right)^2 G \right)^{0.585} - 3 \quad [5]$$

The bulk modulus B of a material is a measure of its hardness and a measure of its resistance to fracture. Shear modulus G measures the resistance to plastic deformation under stress. Young's modulus (E) can be defined as the ratio of tensile stress to tensile strain. These values are shown in Table 2. CoTiP HH compound is a harder compound than other compounds. The fact that CoTiP HH compound is a harder compound than other compounds is due to its Bulk and Young modulus being higher than other CoTiAs and CoTiSb HH compounds. Bulk modulus, Young modulus, and shear modulus values of HH compounds (RhTiP [108], RhCrP [109], RhCrAs [109], RhCrSb [109], RhMnSb [110], CoTiSb [111]) in the literature with F43 m structure are also presented in Table 2. The Bulk modulus values obtained from the structural

parameters presented in Table 1 and the values presented in Table 2 are compatible with each other. Among these HH compounds, the hardest compound is RhCrSb.

The Paugh ratio, known as the ratio of the bulk modulus to the shear modulus, gives information about the covalent/ionic state of the material. The G/B values are given in Table 3. Frequently, G/B is approximately 1.1 for a covalent material, while G/B is 0.6 for an ionic material [108]. Considering these G/B values, CoTiX(X:P, As, Sb) HH compounds are materials with ionic character. Also, RhTiP [108], RhCr(P, As, Sb) [109], and RhMnSb [110] HH compounds have ionic character. On the other hand, the G/B value is one of the determinants in the evaluation of the ductile/brittle property of the material [112]. Otherwise, if this ratio is (0.6 (ductile behavior), it exhibits brittle behavior. From Table 3, CoTiX(X:P, As, Sb) HH compounds exhibit ductile behavior. RhTiP108, RhCr(P, As, Sb)109, and RhMnSb [110] HH compounds have a ductile structure. The Poisson ratio(ν) is a second parameter determining whether the material is ductile/brittle. The critical value for the material to be ductile at this Poisson ratio is ≥ 0.26 [113]. All three compounds CoTiX(X:P, As, Sb), and RhTiP [108], RhCr(P, As, Sb) [109], RhMnSb [110] HH compounds have ν greater than 0.26 as presented in Table 3. Also, the value ν can be used to determine the nature of the central force in the crystal. The lower and upper limits of the Poisson ratio are 0.25 and 0.50, respectively [108]. Generally, $\nu = 0.1$ for covalent materials, while it has a value of 0.25 for ionic materials [108]. CoTiX(X:P, As, Sb) HH compounds show weak ionic properties. Cauchy's pressure ($C' = C_{12}-C_{44}$) is a parameter that defines the angular properties of atomic bonds in metallic structures and compounds, determined from elastic constants [114]. Another detail in the Cauchy pressure is that if the value is positive, the compound shows metallic properties, and its structure is ductile [77]. CoTiX(X:P, As, Sb) and RhTiP [15], RhCr(P, As, Sb) [16], RhMnSb [17] HH compounds show positive C' values, shown in Table 3. The hardness values(Hv) of CoTiP, CoTiAs, and CoTiSb compounds are 11.22 GPa, 9.51 GPa, and 7.52 GPa, respectively. The hardness value of 10 GPa and above is defined as hard [77]. CoTiP HH compound is a hard compound with an Hv value of 11.22 GPa. Among the compounds we compared, RhMnSb has the softest structure with an Hv value of 1.07¹¹⁰. In materials science, plasticity (B/C_{44}) is the irreversible deformation of a solid material against an applied force [115]. As seen in Table 3, All three compounds CoTiX(X:P, As, Sb), and RhTiP [108], RhCr(P, As, Sb) [109], RhMnSb [110] HH compounds have low plasticity.

The Debye temperature θ_D is the critical parameter, and its value can be calculated using the mean sound velocity.

$$\theta_D = \frac{h}{k_B} \left[\frac{3n}{4\pi} \left(\frac{N_A \rho}{M} \right) \right]^{1/3} V_m \quad [6]$$

where h is Planck's constant, k_B is Boltzmann's constant, n is the number of atoms in the cell, N_A is Avogadro's number, M is the molecule mass, ρ is the density, and V_m is the average isotropic sound velocity, which can be expressed as

Table 2

Elastic constants (C_{11} (GPa), C_{12} (GPa), C_{44} (GPa)), Bulk modulus (B(GPa)), Shear modulus (G(GPa)), Young modulus (E(GPa)).

Materials	C_{11}	C_{12}	C_{44}	B	G	E
CoTiP	310.2	125.8	105.8	187.2	100.1	254.8
CoTiAs	278.9	110.6	87.5	166.7	86.1	220.3
CoTiSb	262.2	86.4	61.8	145.0	71.1	183.3
RhTiP [108]	243.7	160.9	90.8	188.6	66.2	177.7
RhCrP [109]	261.1	206.5	108.9	224.6	94.4	35.50
RhCrAs [109]	249.9	184.6	115.8	206.0	71.0	187.0
RhCrSb [109]	400.7	228.0	124.8	285.6	107.8	454.7
RhMnSb [110]	150.0	95.0	40.0	111.9	34.8	94.6
CoTiSb [111]	–	–	–	155.6	–	–

Table 3

G/B ratio, Poisson ratio (ν), Cauchy's pressure(C' (GPa)), Hardness (Hv), Plasticity(B/C_{44}).

Materials	G/B	ν	C'	Hv	B/C_{44}
CoTiP	0.534	0.273	20	11.22	1.76
CoTiAs	0.516	0.279	23	9.51	1.90
CoTiSb	0.490	0.289	25	7.52	2.34
RhTiP [108]	0.351	0.340	70	3.83	2.07
RhCrP [109]	0.421	0.380	98	8.44	2.06
RhCrAs [109]	0.344	0.340	69	3.96	1.77
RhCrSb [109]	0.377	0.420	103	6.88	2.28
RhMnSb [110]	0.310	0.359	55	1.07	2.79

$$V_m = \left[\frac{1}{3} \left(\frac{1}{V_l^3} + \frac{2}{V_t^3} \right) \right]^{-1/3} \quad [7]$$

Here, the longitudinal V_l and transverse V_t sound velocities can be obtained as follows.

$$V_l = \sqrt{\frac{3B + 4G}{3\rho}} \quad [8]$$

$$V_t = \sqrt{\frac{G}{\rho}} \quad [9]$$

The calculated θ_D , V_l , V_t , and V_m are given in Table 4. Debye temperature and sound velocity values of CoTiX(X:P, As, Sb) HH compounds are higher than RhMnSb.

The melting temperature (T_m) is one of the parameters that determine the use of a crystal in heating systems. The melting temperature (T_m) can be calculated using equation [11].

$$T_m = \left[553 K + 5.91 \frac{K}{GPa} x C_{11} \right] \pm 300 K \quad [10]$$

The melting temperature values are given in Table 4. CoTiX(X:P, As, Sb) HH compounds and RhMnSb have very high melting temperatures suitable for high-temperature applications.

Debye temperature is defined by the temperature necessary to activate all the phonon modes for the materials. Compounds with a high melting temperature usually have a high Debye temperature due to stiffer crystal orientation. Also, the high value of Debye temperature shows high energy to excite the phonons, which is more favorable for thermoelectric applications. It can be concluded that CoTiP is a more suitable compound for thermoelectric power generation to obtain clean energy. Debye temperature, melting points, and sound velocities values change as CoTiP > CoTiAs > CoTiSb.

3.3. Anisotropy properties

The control exerted by elastic anisotropy over crucial mechanical properties in solids profoundly impacts their practical applications [116]. The study of material lattice distortion and micro-cracks frequently revolves around understanding the inherent anisotropy of elasticity, making it an indispensable element in material development and utilization. Elastic anisotropy is widely acknowledged for its influence on various phenomena, including phonon modes, phase transformations, dislocation dynamics, crack propagation, and charge defect mobility. Consequently, researchers focusing on materials' mechanical and related physical properties have shown considerable interest in exploring elastic anisotropy. An essential aspect is comprehending how the amalgamation of different chemical species, as seen in high entropy compounds, affects elastic anisotropy, thereby playing a critical role in the engineering of innovative high entropy materials for mechanical applications [117–122].

The elastic anisotropy of the material is significant for understanding the dimensional variation of the mechanical properties of the crystal. The Zener anisotropy index A^Z , the Chung-Buessem anisotropy index A^G , and the universal elastic anisotropy index A^U for a material are proposed as follows Eq.(12)–(14) [123–125].

Table 4

Debye temperature (θ_D), Melting temperature (T_m), Sound velocities (V_m , V_l , V_t).

Materials	θ_D (K)	$T_m \pm 300$ (K)	V_l (m/s)	V_t (m/s)	V_m (m/s)
CoTiP	585.5	2386	7521	4202	4678
CoTiAs	480.0	2201	6407	3543	3947
CoTiSb	399.2	2102	5677	3091	3448
RhMnSb	285.6	1412	4396	2061	2320

$$A^Z = \frac{2C_{44}}{C_{11} - C_{12}} \quad [12]$$

$$A^G = \frac{G_V - G_R}{G_V + G_R} \quad [13]$$

$$A^U = 5 \frac{G_V}{G_R} + \frac{B_V}{B_R} - 6 \geq 0 \quad [14]$$

G_V and B_V are the shear and bulk moduli from the Voigt approximation. Moreover, G_R and B_R are the shear and bulk moduli from the Reuss approach. The crystal is isotropic when the universal an-isotropic index (AU) equals zero. The deviation of this value from zero indicates the level of elastic anisotropy.

The isotropy value of A^Z is 1, and A^G and A^U are zero. Less than or greater than these values define a crystal's elastic anisotropy degree. The $A^G = 1$ defines the maximum elastic anisotropy. In our work, CoTiP and CoTiSb are anisotropic with the anisotropy values ($A^Z = 1.026$, $A^G = 0.000$, and $A^U = 0.000$). On the other hand, CoTiAs is completely isotropic as presented in Table 5.

The VELAS code was used to visualize the effect of anisotropy on mechanical properties in 3D⁶⁹. The deviation from sphericity in the figures drawn with the VELAS code indicates the degree of anisotropy in the three-dimensional mechanical properties.

As seen Fig. 2 and Table 6, CoTiAs is isotropic in all mechanical properties. CoTiP and CoTiSb are anisotropic in all other mechanical properties (young modulus E(GPa), shear modulus G(GPa), and Poisson's ratio (v)) except linear compression (β (TPa⁻¹)). In Fig. 2, the yellow color indicates the minimum, whereas the green color signifies the maximum.

3.4. Electronic properties

The electronic properties of any material give information about the nature of the material. The electronic properties' precision causes the compound's physical properties to be exact. The energy band structure along the high symmetry direction(WLFXWK) is presented in Fig. 3 with the total electronic state density to investigate the electronic structure and phase stability of the CoTiX(X:P, As, Sb) HH compounds. As seen in Fig. 3, the maximum valence band of the CoTiX(X:P, As,Sb) HH compounds is at the Γ point and the conduction band minimum is at the X point. The Fermi level is set at 0 ev. Since there is no overlap between the valence and conduction bands at the Fermi levels, it indicates a semiconductor with an indirect band gap. The band gap values of the compounds are 1.402 eV (CoTiP), 1.232 eV (CoTiAs) and 1.003 eV (CoTiSb).

One of the critical elements in improving the characteristics of alloys is electronegativity. Electronegativity serves as a bridge for electrons to travel to the most electronegative element. As we know, the ability of a semiconductor to transfer photoexcited electrons to species adsorbed on its surface is governed by the band energy position of the semiconductor and the redox potentials of the adsorbate, which is related to electronegativity. A bond's ionic and covalent character can be determined by the electronegative difference between two bonded atoms [126]. Significant differences provide an ionic bond due to charge transfers between atoms. By contrast, minor differences feature covalent bonds due to charge sharing. According to Duffy [127] there is a relationship between band gap and electronegativity, as expressed by

$$v_{max} = 30000[\chi_{opt}(anion) - \chi_{opt}(metal ion)] \quad [15]$$

Where v_{max} is the onset of optical absorption, χ_{opt} is the optical electronegativity. The decrease of band gap is accompanied by a decrease of ionicity in bonding, which arises from a decreased electronegativity difference. Verma [128] found a linear relationship between the band gap and the optical electronegativity of solids. As the electronegativity difference between the elements decreases, the band gap decreases. The band gap values of CoTiX(X: P, As, Sb) HH compounds decrease from P

Table 5
Anizotropy parameters.

	G _V (GPa)	B _V (GPa)	G _R (GPa)	B _R (GPa)	A ^Z	A ^G	A ^U
CoTiP	100.36	187.27	99.905	187.27	1.147	0.002	0.022
CoTiAs	86.16	166.7	86.128	166.7	1.026	0.000	0.000
CoTiSb	72.24	145	71.185	145	0.703	0.007	0.0741

to Sb. Since Co and Ti elements are in all three compounds, the Pauli electronegativity values of P, As, and Sb elements are 2.19, 2.18, and 2.05, respectively. RhCr(P, As, Sb) [109] and RhTiP [108] compounds are formed at the valence band maximum and conduction band minimum at Γ X points, and they are indirect band semiconductor HH compounds.

A review of Cobalt (Co)-based compounds established that the band gaps of the examined compounds fell within the range of 0.03–1.13 eV. It was concluded that compounds within this range exhibit favorable thermoelectric properties [129]. In our study, it can be asserted that Cobalt Titanium Antimonide (CoTiSb) possesses a band gap within the specified range, suggesting its potential as a promising thermoelectric material.

When we included the spin-polarized contribution for the electronic band structure calculations, the compounds we examined for the current pseudopotential did not exhibit magnetic properties because the total magnetic moment was zero. As a result, we did not include the spin-polarizing effect. Wang et al. [130] have determined the magnetic ground state structure of Sr₂CuFe₆ under collinear magnetic configuration as a ferromagnetic configuration due to lower energy. They obtained a spin-polarized band structure for ferromagnetic Sr₂CuFe₆ and found that the bands in the spin-up direction exhibit a semiconducting behavior with a large energy gap of 4.34 eV. Meanwhile, the bands in the spin-down direction exhibit a metallic behavior and overlap with the Fermi level. Contrary to Ref. [130], it can be seen that the spin-polarized electronic band structure of BaNi₂O₆ exhibits metallic behavior for the spin-up bands due to overlap with E_F. However, it shows semiconducting behaviors since E_F is located between the large gap (~1.09 eV) for the spin-down bands [131].

Partial DOS of the CoTiX(X:P, As, Sb) HH compounds are also shown in Fig. 4. We can analyze the graph given in Fig. 4 in the valence band, Fermi level, and conductivity band. The band gap near the Fermi level is due to the d band of Co and Ti atoms, mainly indicating that the d states of Co and Ti play an essential role in the physical properties of CoTiX compounds. In the valance region near the 3eV, the contribution of p-states for Sb is higher than P and As. Generally, DOS values in the valance and conductivity region are higher for CoTiSb.

3.5. Vibrational properties

The vibrational intensity of states of cubic CoTiX(X:P, As, Sb) HH compounds is presented in Fig. 5. Phonon frequencies were obtained using the Phonopy code with the $2 \times 2 \times 2$ supercell approach without SOC as seen in Refs. [132–135]. We used the density functional perturbation theory to obtain the force constants. Since there are three atoms in the primitive cell of CoTiX(X:P, As, Sb) HH compounds, there are nine phonon modes for any wave vector. Three phonon modes are acoustic, and the other six are optical. The determined phonon distribution curves of CoTiX(X: P, As, Sb) indicate that they are dynamically stable in the MgAgAs structure, as there are no negative phonon modes for all three HH compounds. Phonon modes, regarded as normal modes or quantum units of vibrations within crystals, play a crucial role in maintaining the stability of crystal structures. The stability of phonons hinges upon the essential criterion that the frequency associated with each phonon must be a real quantity rather than an imaginary one [129].

In Fig. 5, there are acoustic branches in the low-frequency region (longitudinal acoustic (LA) mode and two transverse acoustic (TA)

modes) and optical branches in the high-frequency region (three longitudinal optical (LO) modes and three transverse optical (TO) modes). In Fig. 5, for the compounds, the optical and acoustic modes are disturbed separately at the second Γ point and have symmetry concerning this point except CoTiAs as K₈Si₄₆ [134]. In Fig. 5, the determined optical frequency values(Thz) are 9.98, 9.81 for CoTiP, 7.41, 8.26 for CoTiAs and 6.82, 7.47 for CoTiSb. At low frequencies, around the Γ point, the dispersion curve's or group velocity slope in acoustic modes is higher than in optical modes. As a result, thermal energy is transferred mainly by acoustic modes [136]. The transverse acoustic (TA) modes provide valuable insights into the thermal conduction characteristics of a compound. A lack of scattering in the TA modes indicates high thermal conductivity in the compound.

Scattering may occur due to degeneracy or interfusion between the transverse optical (TO) and TA modes. Specifically, if the frequency values of the TO modes are lower than those of the TA modes, scattering of the TA modes can occur. The occurrence of scattering reduces thermal conductivity, resulting in a lower thermal conductivity for the compound [137]. In the case of CoTiX (X: P, As, Sb), as illustrated in Fig. 5, there is no interfusion between the TO and TA modes, affirming the high thermal conductivity of this alloy [138]. The band gaps between the optical and acoustic modes are due to the triatomic structure (difference in atomic masses). Since the mass difference from P element to Sb increases in the periodic table, the acoustic and optical modes are widened [139]. The phonon gap for CoTiSb is wider than CoTiP. In X symmetry points, a sixfold degenerate phonon band crossing with linear dispersion can be seen (see Fig. 5), as similar behavior was also found in Ref. [134].

3.6. Optical properties

The optoelectronic behaviors of CoTiX(X: P, As, Sb) HH compounds were analyzed in the 0–50 eV range by determining the optical properties. Optical properties are significant for semiconductor materials; it explains the relationship between electronic band structure and optical properties [77]. Also, in the optical properties of semiconductor materials, metal-like behavior is observed at very low frequencies, while it exhibits an insulating behavior at very high frequencies [140]; this requires examining optical properties with changes in incident photon energy. The dielectric function can obtain optical properties, such as refractive index, extinction coefficient, reflectivity, conductivity, and absorption coefficient. The dielectric function for a material explains the interaction of photons incident on the material and electrons in the material; hence, it is a linear system response to incoming electromagnetic radiation [141,142]. The complex dielectric function is defined by Ehrenreich and Cohen's equations [143].

$$\epsilon(\omega) = \epsilon_1(\omega) + i\epsilon_2(\omega) \quad [16]$$

The first term in the equation $\epsilon_1(\omega)$ is the real part giving the propagation properties, the second term $i\epsilon_2(\omega)$ is the imaginary part responsible for optical absorption in a medium. The real and imaginary components of the frequency-dependent dielectric function have been calculated using the Kramers–Kronig relations [37].

Fig. 6 presents a separate plot of the real and imaginary parts of the calculated dielectric function of CoTiX(X:P, As, Sb) HH alloys according to the photon energy in the range of 0–15 eV (the point of change is focused). The real part of the dielectric function can be explained by the Penn model [144], where $\epsilon_1(0)$ gives larger values of $\epsilon_1(0)$ despite the smaller band gap. The static real part $\epsilon_1(0)$ of dielectric constant for

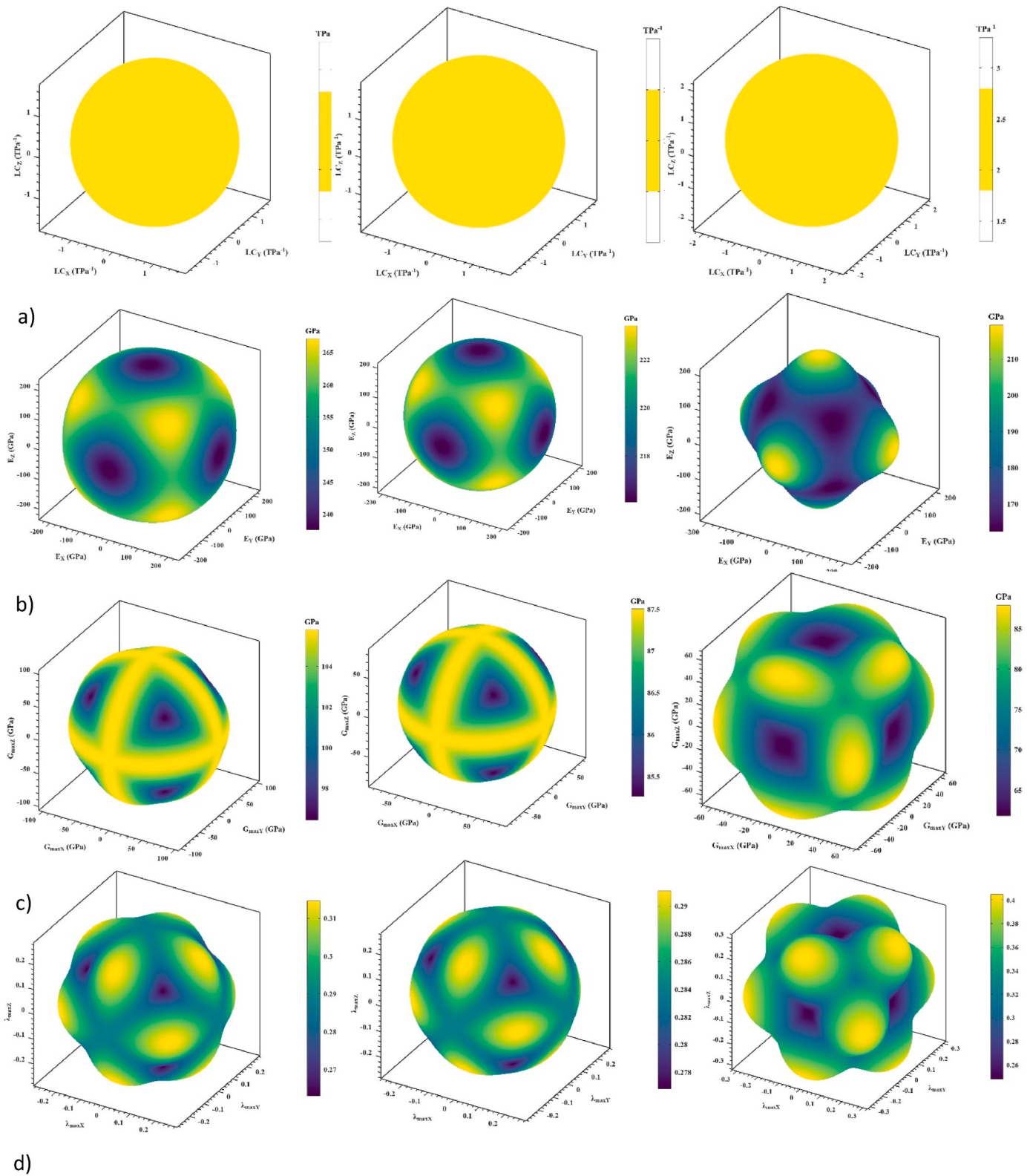


Fig. 2. Elastic modules in 3D: a) linear compression (β (TPa^{-1})), b) young modulus E(GPa), c) shear modulus G(GPa) d) Poisson's ratio (ν)) of CoTiP, CoTiAs, CoTiSb, respectively.

CoTiP, CoTiAs and CoTiSb are 19.49, 20.30 and 21.02. The value of $\varepsilon_1(\omega)$ increased from P to Sb, which can be explained by the decrease in atomic diameters from Sb to P [145]. Static dielectric constant values [146] for CoFeX(P, As, Sb) and XCoSb(Ti, Zr, Hf) Half Heusler compounds with similar structures are between 18 and 22 values 145 and.

The frequency at which the material transitions to a metallic dielectric is called the plasma frequency. (ω_p) and is defined as the frequency at which the real part of the dielectric function is lost at $\varepsilon_1(\omega_p) = 0$ [147]. The values of ω_p are 3.42 eV (CoTiSb), 3.54 eV (CoTiAs), and 3.76 eV (CoTiP). While $\varepsilon_1(\omega)$ values show that energy absorption is high in the

Table 6

The minimum and maximum values of mechanical properties.

Material	β (TPa $^{-1}$)		G(GPa)		E(GPa)		D	
	β_{\min}	β_{\max}	G $_{\min}$	G $_{\max}$	E $_{\min}$	E $_{\max}$	v $_{\min}$	v $_{\max}$
CoTiP	1.78	1.78	92.2	105.8	237.61	267.1	0.224	0.314
Anisotropy	1.0		1.148		1.124		1.402	
CoTiAs	1.99	1.99	84.15	87.50	216.09	223.41	0.265	0.291
Anisotropy	1.0		1.04		1.034		1.098	
CoTiSb	2.29	2.29	61.8	87.9	162.34	219.37	0.196	0.404
Anisotropy	1.0		1.422		1.351		2.061	

IR and visible regions, the values decrease to a minimum when passing from Visible to the UV region. Negative $\varepsilon_1(\omega)$ values indicate that the electromagnetic radiation on the surfaces of CoTiX HH compounds is reduced, metallic behavior is dominant in the visible and UV regions [148]. Therefore, these HH compounds have uses in optical filters or shielding devices in different frequency regions. The imaginary part of the dielectric function shows the optical transitions between the valence band and the conduction band and determines that the studied materials are semiconductors. Two types of transitions contribute to the dielectric function: intra-band and inter-band (direct and indirect). While the intra-band transition is seen in metals, since our compounds are semiconductors [145], the inter-band transition is seen. The value of the dielectric function at zero frequency is the optical band gap of the compound. The calculated values are 1.41 eV(CoTiP), 1.32 eV(CoTiAs), and 1.17(CoTiSb) eV. The optical band gap and band gap values in electronic calculations are compatible. The optical band gaps are 0.775 eV, 1.102 eV, and 1.156 eV for TiCoSb, ZrCoSb, and HfCoSb HH compounds, respectively [145]. The prominent peaks for the imaginary dielectric function $\varepsilon_2(\omega)$, are observed at 2.58 eV (CoTiP), 2.21 eV (CoTiAs), and 1.95 eV (CoTiSb). The peaks in $\varepsilon_2(\omega)$ show a fluctuating characteristics in visible region and IR. The positive values of $\varepsilon_2(\omega)$ indicate regions of optical absorption [149].

The complex refractive index combines the real $n(\omega)$ and the imaginary part $k(\omega)$. $n(\omega)$ is the simple refractive index, and $k(\omega)$ is the extinction coefficient [150]. The refractive index serves as a crucial optical parameter, quantifying the velocity of light within a substance relative to its speed in a vacuum. Simultaneously, the extinction coefficient gauges how much the material dissipates light energy [151]. The refractive index $n(\omega)$ as a function of photon energy is presented in Fig. 7a for CoTiX(X:P,As,Sb) HH compounds. The values of $n(\omega)$ at zero frequency are 4.43, 4.50, and 5.80 for CoTiP, CoTiAs, and CoTiSb, respectively. The elevated refractive index of CoTiX (X: P, As, Sb) renders it valuable in the fabrication processes of fibers and optical filters [151]. The relatively large refractive index values result from the small band gap [152]. The highest peaks of refraction are in the IR and visible regions, and there is a decrease in the peaks towards the ultraviolet region. The presence of peaks in the visible regions is due to interband transitions between the top of the valence band and the bottom of the conduction band [153–155]. The extinction coefficient $k(\omega)$ of CoTiX(X: P,As,Sb) HH compounds with respect to energy is plotted in Fig. 7b. The maximum peaks for extinction coefficient $k(\omega)$ are 4.52 (CoTiP), 4.72 (CoTiAs), and 4.26 (CoTiSb). The behavior of $k(\omega)$ against energy values is similar to $\varepsilon_2(\omega)$, because $k(\omega)$ value is a measure of the absorption of radiation incident on the compound.

The reflection coefficient, $R(\omega)$, refers to the amount of electromagnetic radiation reflected from the incoming surface. Its variation against energy is presented in Fig. 7c. It is seen from the graph that there is a reflection between 0 and 15 eV for all compounds, but it gradually decreases and goes to zero around 40 eV.

The loss function, $L(\omega)$, represents the energy loss of a fast electron passing through the material [156], and its variation against energy is presented in Fig. 7d. The peaks in the loss function plot are associated with the plasma resonance, called the plasma frequency ω_p , and are shown in Fig. 7d. Plasma frequency values are 3.11(CoTiP), 3.03

(CoTiAs) and 2.90 (CoTiSb). $L(\omega)$ values in the 0–10 eV range and 35–50 eV are minimal. Small values indicate that the energy loss is low.

The variation of the absorption coefficient $\alpha(\omega)$ with energy is presented in Fig. 7e. When the graph was examined, it peaked around 10 eV (infrared region) for the three compounds and decreased with increasing energies. The presence of high values in the absorption coefficient is interband absorption in semiconductor compounds [157].

3.7. Thermodynamic properties

The effects of CoTiX HH compounds on thermodynamic properties when exposed to high temperature and high pressure were investigated. Thermal properties were calculated with the quasi-harmonic Debye model in Gibbs code [158]. The thermodynamic properties are analyzed in the 0–1000 K temperature range and the pressure range of 0–30 GPa for CoTi (P, As) and 0–25 GPa for CoTiSb. Temperature and pressure effects on bulk modulus (B), volume (V), Debye temperature (θ_D), Gruneisen parameter (γ), thermal expansion (α), and heat capacity (Cv) are shown in Figs. 8 and 9.

The change in volume of CoTiX HH compounds according to the pressure at different temperatures is shown in Fig. 8a. We can see that, at a given temperature, the volume decreases when the pressure increases. On the other hand, at a given pressure, the volume increases with temperature at a prolonged rate. At a given temperature, the volume decreases as the pressure increases, while at a given pressure, the volume decreases at a prolonged rate with temperature. In other words, it was determined that the effect of pressure on the compounds was significant.

The pressure and temperature dependence of the bulk modulus of CoTiX (X: P, As, Sb) compounds are shown in Fig. 8b. Bulk modulus values decrease with increasing temperature at a specific pressure. On the other hand, it increases with increasing pressure at a specific temperature. The increase in the bulk modulus values of the compound indicates its compressibility. The same trend is confirmed for many Heusler compounds [159–162]. The calculated bulk moduli are 180.04 (CoTiP) GPa, 161 (CoTiAs) GPa, and 140 (CoTiSb) GPa at zero temperature and zero pressure. The bulk modulus values calculated from the structural properties are compatible with 184.04 GPa (CoTiP), 164.3 GPa (CoTiAs), and 142.8 GPa (CoTiSb). Also, at 300 K and zero pressure, the bulk modulus is 172.82 (CoTiP) GPa, 153.03 (CoTiAs) GPa, and 134.40 (CoTiSb) GPa. In light of these values, it can be said that the studied compounds are significantly compressible, and especially CoTiP is harder than the others [162]. Numerous studies [163,164] have consistently validated a robust association between hardness and the Bulk modulus value. This correlation suggests that the Bulk modulus is intricately linked to the rigidity of the material's network, with hard substances consistently exhibiting elevated Bulk modulus values and displaying resistance to plastic deformation.

The Debye temperature, θ_D , provides valuable information about the different physical properties of solids, such as elastic constants, specific heat, and melting temperature [165]. The relationship between Debye temperature (θ_D) and temperature in the pressure range 0–30 GPa for CoTi(P, As) and 0–25 GPa for CoTiSb is presented in Fig. 8c. Debye temperature values decrease as the temperature increases at a specific

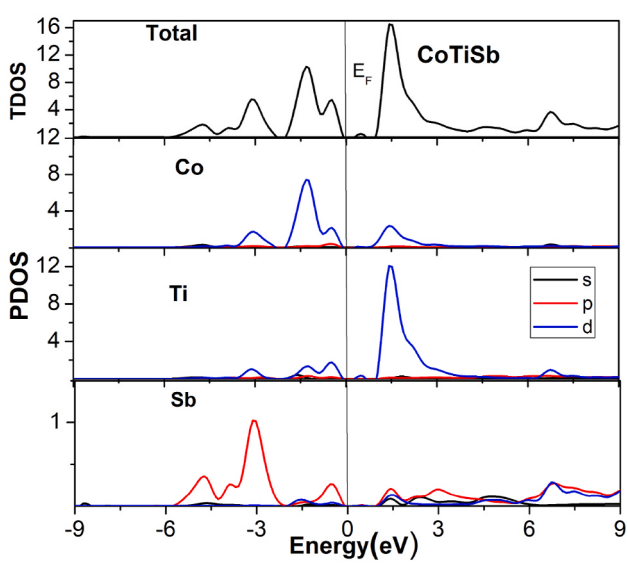
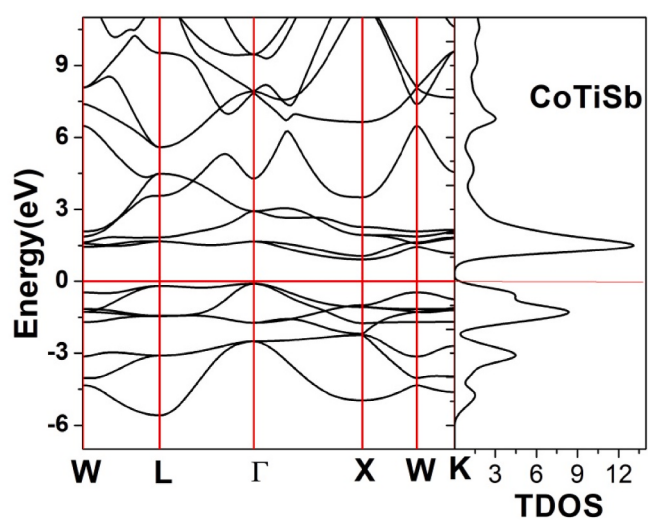
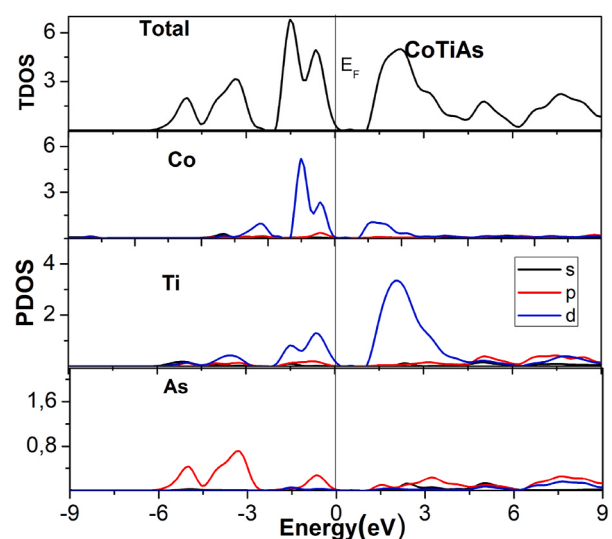
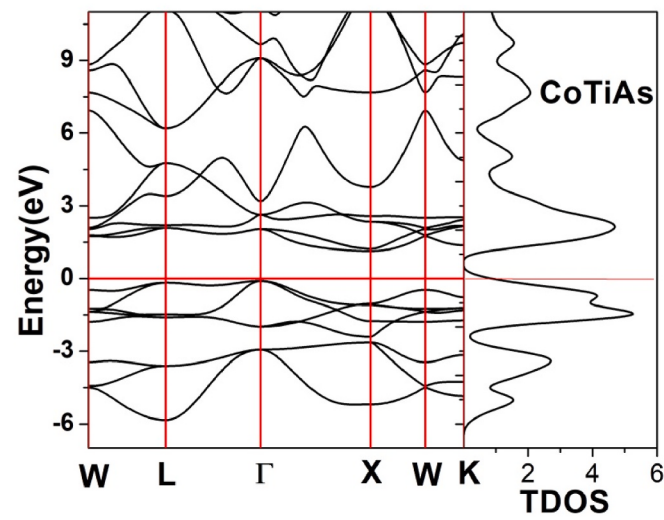
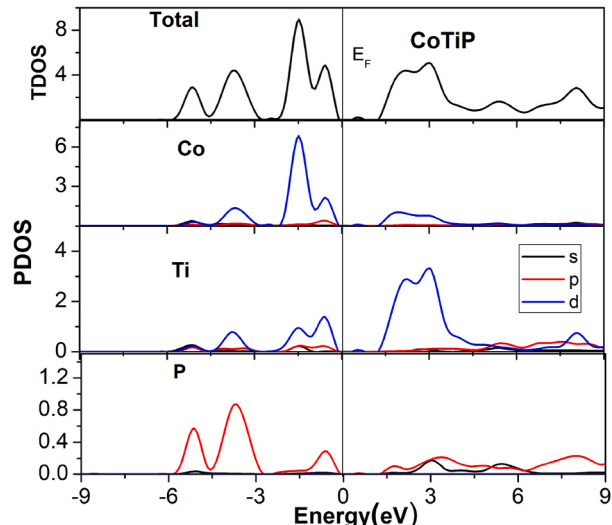
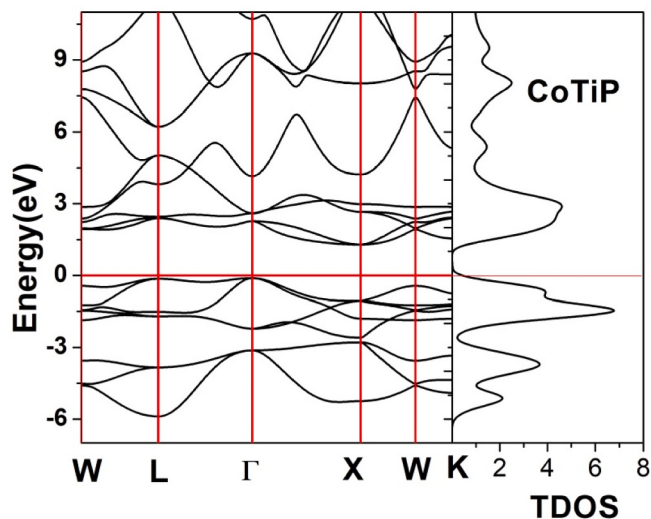


Fig. 3. Electronic band structure and total density of CoTiX(X:P,As,Sb) HH compounds.

Fig. 4. Partial density of states of CoTiX(X:P,As,Sb) HH compounds.

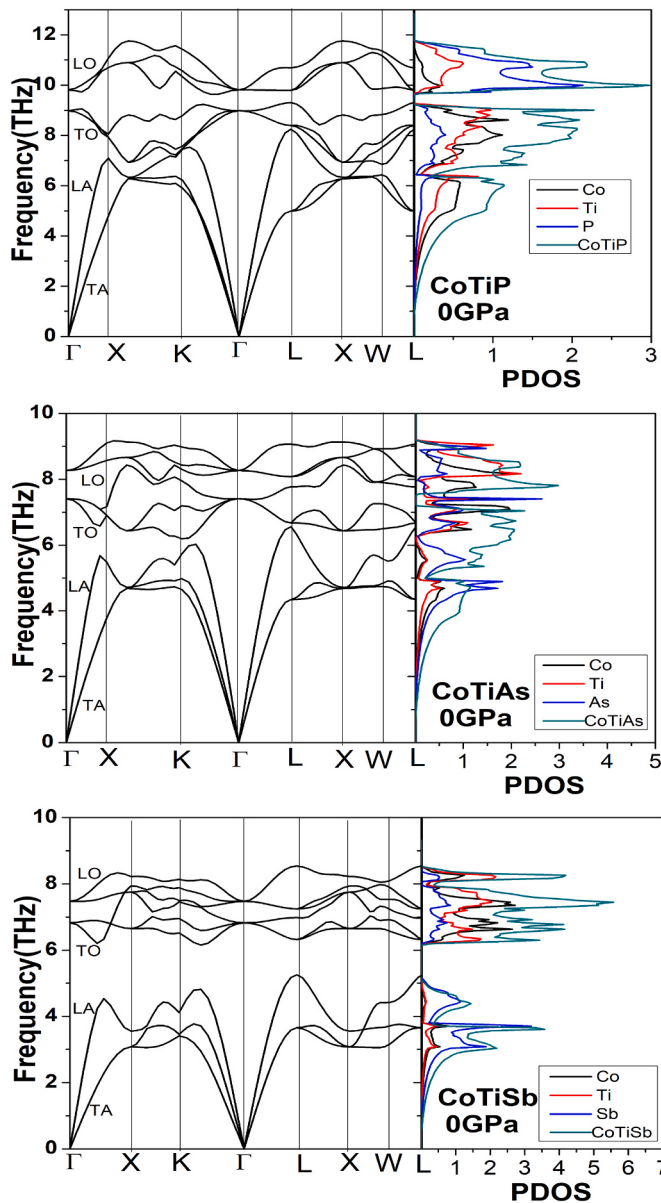


Fig. 5. The phonon dispersion curves and phonon DOS for $\text{CoTiX}(\text{X:P, As, Sb})$ HH compounds.

pressure value, on the other hand, it increases as the pressure increases at a particular temperature value. The effect of pressure on Debye's temperature is much greater than temperature. The same effect was observed in the NgAgSi HH compound [161]. Debye temperature values calculated at 300 K and 0 GPa are 567.24 K, 473.07, and 386.68 K for CoTiP , CoTiAs , and CoTiSb HH compounds, respectively. The compounds have high Debye temperatures, resulting in high thermal conductivity and melting point [166], which are the high melting temperatures of the compounds obtained from the elastic parameters.

Gruneisen parameter, one of the thermodynamic parameters, is related to anharmonic vibrations. Anharmonicity in phonon frequencies is related to volume. The change in the Gruneisen parameter of CoTiX (X: P, As, Sb) HH compounds according to the pressure at different temperatures is shown in Fig. 8d. While this parameter is almost constant at $0 \leq V \leq 200$ K at specific pressure values, it increases after 200 K. On the other hand, when the temperature is constant, it decreases with the increase in pressure. A decrease in the value of the Gruneisen parameter indicates a decrease in anharmonic, which increases the thermal conductivity [161].

Thermal expansion (α), one of the thermodynamic parameters, is related to melting temperature, anharmonicity, and bond strength. The thermal expansion coefficients of the compounds were calculated as seen in Fig. 9a, which is that the material changes its physical properties in response to a change in temperature, usually excluding phase transitions. It was observed that the coefficients of thermal expansion for all three compounds increased exponentially with the increase in temperature for specific pressure values. An increase in the coefficient of thermal expansion means a weak bond and lower melting point [167].

The temperature and pressure relationship of the heat capacities (C_v) is given in Fig. 9b. C_v values increase rapidly with temperature up to 300 K and are proportional to T^3 [168]. At temperatures higher than 300 K, the increase slowed down and stabilized, reaching the Petit and Dulong limit [162], which is typical for all solids at high temperatures [169]. The heat capacity values we calculated for the compounds at 900 K and 0 GPa are 73.51 J/mol-K, 73.92 J/mol-K, and 74.21 J/mol-K for CoTiP , CoTiAs and CoTiSb compounds, respectively.

4. Conclusion

Some theoretical calculations of CoTiX (X:P, As, Sb) HH compounds have been investigated using the plane wave plane-wave pseudopotential approach in DFT within the GGA approximation. HH compounds have ductile and ionic character and have a stable structure, as demonstrated by elastic, structural, and mechanical properties. The electronic analysis shows these compounds are semiconductors with small indirect band gaps at $\Gamma - \text{X}$ symmetry points. The phonon

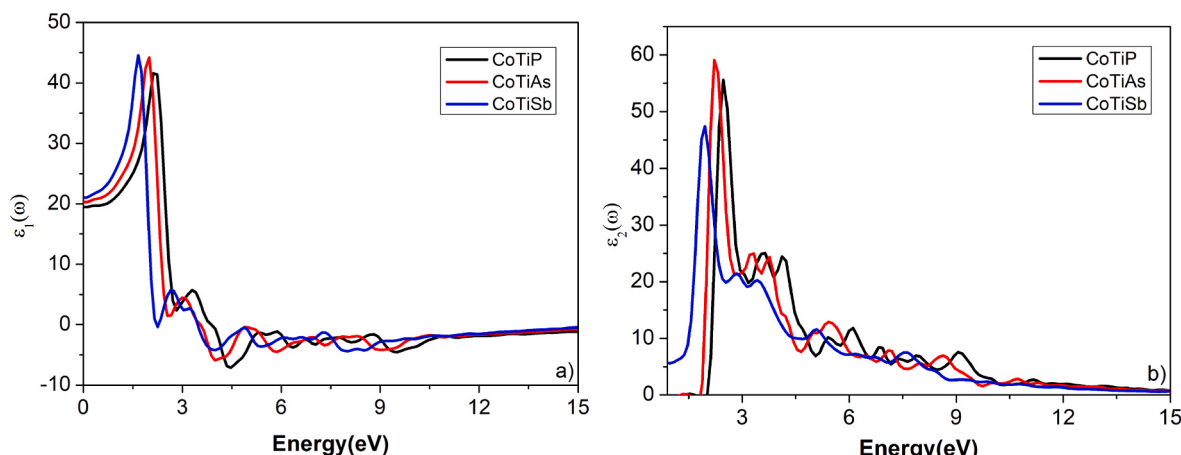


Fig. 6. Dielectric function of a) real and b) imaginary part of $\text{CoTiX}(\text{X:P, As, Sb})$ HH compounds.

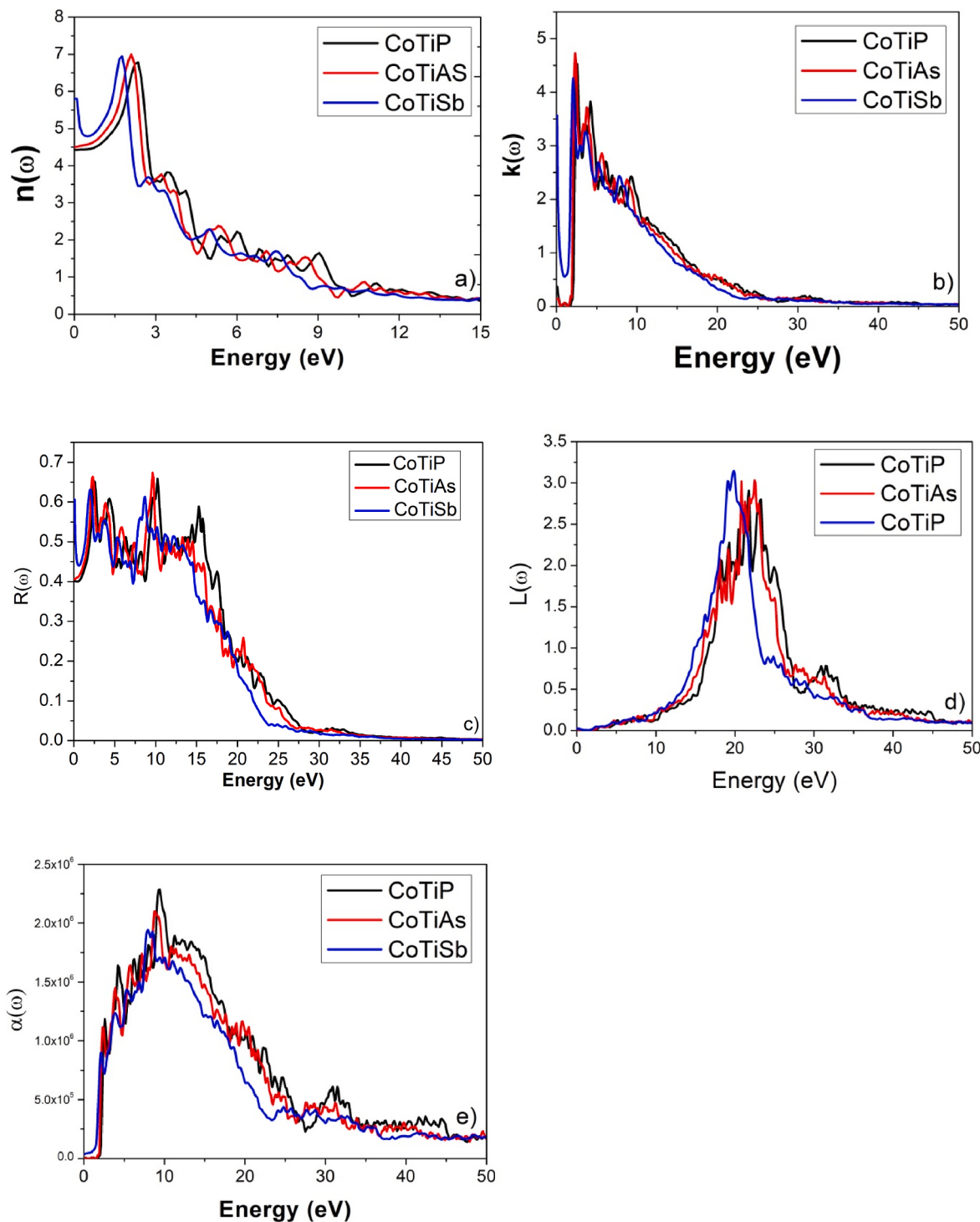


Fig. 7. Optic parameters of (a)–(e) CoTiX(X:P, As, Sb) HH compounds as a function of the energy.

vibration calculations show that all three HH compounds are dynamically stable, with the acoustic and optical band gap increasing from the P to Sb element. The effects of pressure and temperature on thermodynamic properties such as bulk modulus (B), volume (V), Debye temperature (θ_D), Gruneisen parameter (γ), thermal expansion (α), and heat capacity (C_V) have been studied in detail. CoTiX compounds are semiconductors, have high melting temperatures, and show good optical conductivity and reflectivity in various regions of the electromagnetic spectrum. These compounds are suitable materials for high-temperature applications and optoelectronic devices.

CRediT authorship contribution statement

Ilknur Kars Durukan: Conceptualization, Data curation, Investigation, Writing – original draft, Writing – review & editing. **Yasemin Oztekin Ciftci:** Methodology, Software, Writing – review & editing. **Hatice Tekin:** Writing – review & editing.

Declaration of competing interest

The authors declare that they have no known competing financial

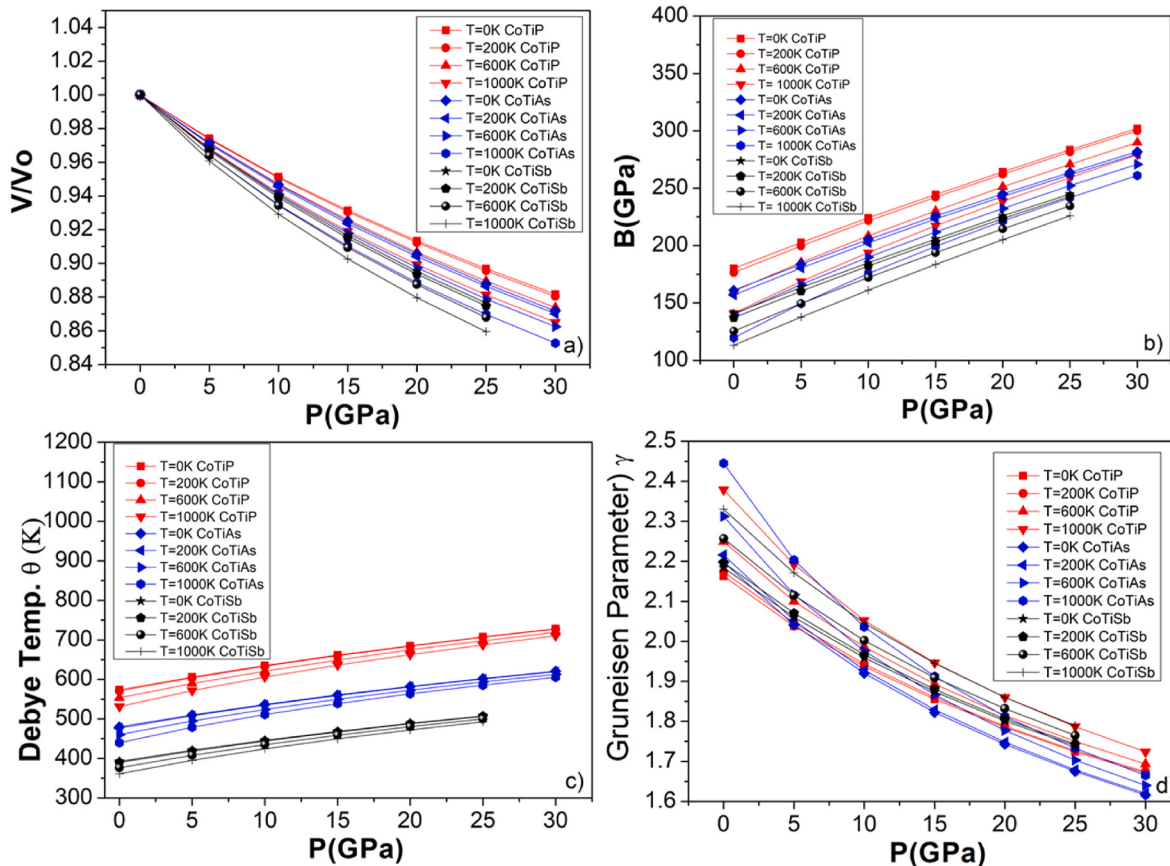


Fig. 8. The variations of a) V/V_0 , b) Bulk modulus, c) Debye temperature, d) Gruneisen parameter with pressure at different temperatures for CoTiX (X: P, As, Sb) HH compounds.

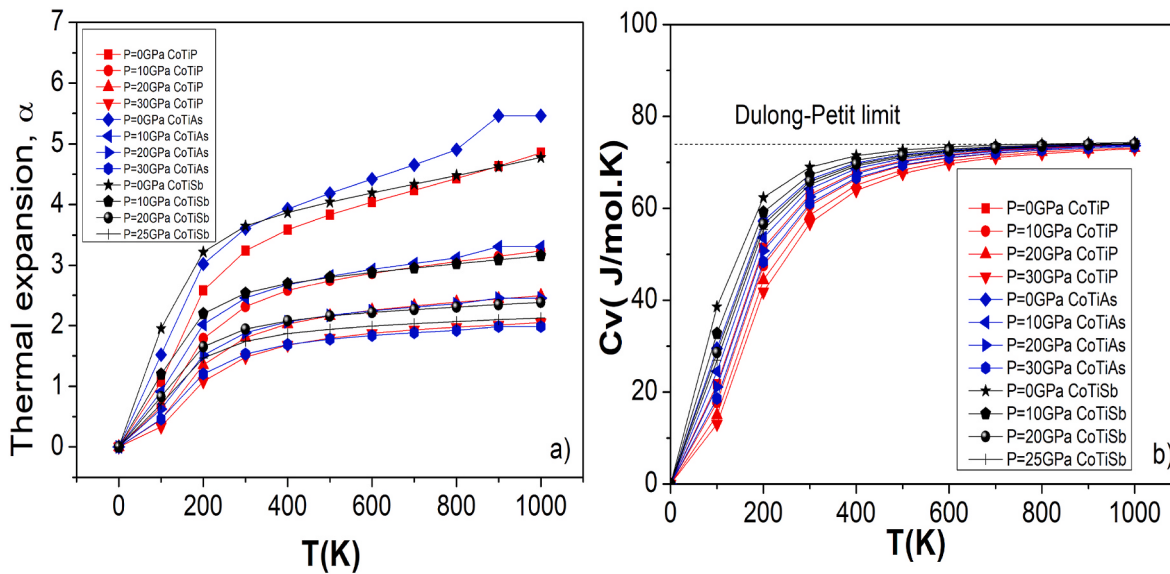


Fig. 9. The variations of a) Thermal expansion b) C_v with the temperature at different pressures for CoTiX (X: P, As, Sb) HH compounds.

interests or personal relationships that could have appeared to influence the work reported in this paper.

Data availability

The data that has been used is confidential.

Acknowledgments

This research is supported by a grant from The Scientific Research Project of Gazi University, Turkey (BAP, Grant No: 7468).

References

- [1] S. Guo, Y. Zhang, Y. Ge, S. Zhang, H. Zeng, H. Zhang, 2D V-V binary materials : status and challenges 1902352 (2019) 1–19, <https://doi.org/10.1002/adma.201902352>.
- [2] M. Goyal, M.M. Sinha, Effect of spin-orbital coupling on the electronic, mechanical, thermoelectric, and vibrational properties of $X\text{PtBi}$ ($X = \text{Sc}$ and Y): a first-principles study, *J. Phys. Chem. Solid.* 153 (February) (2021), <https://doi.org/10.1016/j.jpcs.2021.110024>.
- [3] K. Hamaya, M. Yamada, Semiconductor spintronics with Co 2 - heusler compounds, *MRS Bull.* 47 (6) (2022) 584–592, <https://doi.org/10.1557/s43577-022-00351-0>.
- [4] J.K. Kawasaki, S. Chatterjee, P.C. Canfield, Full and half - heusler compounds, *MRS Bull.* 47 (6) (2022) 555–558, <https://doi.org/10.1557/s43577-022-00355-w>.
- [5] S. Jiang, Review of high-throughput computational design of Heusler alloys, *J. Alloys Compd.* 867 (2021) 158854, <https://doi.org/10.1016/j.jallcom.2021.158854>.
- [6] T. Jin, Y. Jung, Recent progress in computational discovery of Heusler alloys, 2022, pp. 484–491, <https://doi.org/10.1002/bkcs.12484>.
- [7] S. Tavares, K. Yang, M.A. Meyers, Progress in Materials Science Heusler alloys : past , properties, new alloys, and prospects, *Prog. Mater. Sci.* 132 (September 2022) (2023) 101017, <https://doi.org/10.1016/j.pmatsci.2022.101017>.
- [8] W.Y.S. Lim, D. Zhang, S.S.F. Duran, et al., A systematic approach for semiconductor half-heusler, *Front. Mater.* 8 (November) (2021) 1–8, <https://doi.org/10.3389/fmats.2021.745698>.
- [9] A. Roy, J.W. Bennett, K.M. Rabe, D. Vanderbilt, Half-heusler semiconductors as piezoelectrics, *Phys. Rev. Lett.* 109 (3) (2012) 1–5, <https://doi.org/10.1103/PhysRevLett.109.037602>.
- [10] D.M. Hoat, M. Naseri, Electronic and thermoelectric properties of RbYSn half-Heusler compound with 8 valence electrons: spin-orbit coupling effect, *Chem. Phys.* 528 (August 2019) (2020) 110510, <https://doi.org/10.1016/j.chemphys.2019.110510>.
- [11] D. Shrivastava, S.P. Sanyal, Theoretical study of structural, electronic, phonon and thermoelectric properties of KScX ($X=\text{Sn}$ and Pb) and KYX ($X=\text{Si}$ and Ge) half-Heusler compounds with 8 valence electrons count, *J. Alloys Compd.* 784 (2019) 319–329, <https://doi.org/10.1016/j.jallcom.2019.01.050>.
- [12] A. Dey, R. Sharma, S.A. Dar, An extensive investigation of structural, electronic, thermoelectric and optical properties of Bi-based half-Huesler alloys by first-principles calculations, *Mater. Today Commun.* 25 (September) (2020) 101647, <https://doi.org/10.1016/j.mtcomm.2020.101647>.
- [13] A. Candan, A.K. Kushwaha, A first-principles study of the structural, electronic, optical, and vibrational properties for paramagnetic half-Heusler compound TiIrBi by GGA and GGA + mBJ functional, *Mater. Today Commun.* 27 (December 2020) (2021), <https://doi.org/10.1016/j.mtcomm.2021.102246>.
- [14] D.M. Hoat, Electronic structure and thermoelectric properties of Ta-based half-Heusler compounds with 18 valence electrons, *Comput. Mater. Sci.* 159 (December 2018) (2019) 470–477, <https://doi.org/10.1016/j.commatsci.2018.12.039>.
- [15] P.O. Adebambo, R.O. Agbaoye, A.A. Musari, B.I. Adetunji, G.A. Adebayo, Band structure, thermoelectric properties, effective mass and electronic fitness function of two newly discovered 18 valence electrons stable half-Heusler $\text{TaX}(\text{X}=\text{Co},\text{Ir})\text{Sn}$ semiconductors: a density functional theory approach, *Solid State Sci.* 100 (December 2019) (2020) 106096, <https://doi.org/10.1016/j.solidstatesciences.2019.106096>.
- [16] Z. Liu, S. Guo, Y. Wu, et al., Design of high-performance disordered half-heusler thermoelectric materials using 18-electron rule, *Adv. Funct. Mater.* 29 (44) (2019), <https://doi.org/10.1002/adfm.201905044>.
- [17] T. Fang, X. Zhao, T. Zhu, Band structures and transport properties of high-performance half-heusler thermoelectric materials by first principles, *Materials* 11 (5) (2018), <https://doi.org/10.3390/ma11050847>.
- [18] S. Sakurada, N. Shutoh, Effect of Ti substitution on the thermoelectric properties of $(\text{Zr,Hf})\text{NiSn}$ half-Heusler compounds, *Appl. Phys. Lett.* 86 (8) (2005) 1–3, <https://doi.org/10.1063/1.1868063>.
- [19] D. Kieven, R. Klenk, S. Naghavi, C. Felser, T. Gruhn, I-II-V half-Heusler compounds for optoelectronics: ab initio calculations, *Phys. Rev. B Condens. Matter* 81 (7) (2010) 1–6, <https://doi.org/10.1103/PhysRevB.81.075208>.
- [20] A. Hirohata, J. Sagar, L. Lari, L.R. Fleet, V.K. Lazarov, Heusler-alloy films for spintronic devices, *Appl. Phys. Mater. Sci. Process* 111 (2) (2013) 423–430, <https://doi.org/10.1007/s00339-013-7679-2>.
- [21] Singh C. Pallavi, P.K. Kamlesh, R. Gupta, A.S. Verma, Thermoelectric performance of cadmium-based LiCdX ($X = \text{N, P, As, Sb}$ and Bi)-filled tetrahedral semiconductors: applications in green energy resources, *Pramana - J. Phys.* 97 (4) (2023), <https://doi.org/10.1007/s12043-023-02627-9>.
- [22] P.K. Kamlesh, R. Agarwal, U. Rani, A.S. Verma, First-principles calculations of inherent properties of Rb based state-of-the-art half-Heusler compounds: promising materials for renewable energy applications, *Phys. Scripta* 96 (11) (2021), <https://doi.org/10.1088/1402-4896/ac119d>.
- [23] P.K. Kamlesh, Kumari S. Pravesh, A.S. Verma, Effect of hybrid density functionals on half-Heusler LiZnX ($X = \text{N, P}$ and As) semiconductors: potential materials for photovoltaic and thermoelectric applications, *Phys. Scripta* 95 (9) (2020), <https://doi.org/10.1088/1402-4896/abab36>.
- [24] P.K. Kamlesh, R. Agrawal, U. Rani, A.S. Verma, Comprehensive ab-initio calculations of AlNiX ($X = \text{P, as and Sb}$) half-Heusler compounds: stabilities and applications as green energy resources, *Mater. Chem. Phys.* 275 (September 2021) (2022) 125233, <https://doi.org/10.1016/j.matchemphys.2021.125233>.
- [25] P. Verma, C. Singh, P.K. Kamlesh, K. Kaur, A.S. Verma, Nowotny-Juza phase KBeX ($X = \text{N, P, As, Sb, and Bi}$) half-Heusler compounds: applicability in photovoltaics and thermoelectric generators, *J. Mol. Model.* 29 (1) (2023) 19–22, <https://doi.org/10.1007/s00894-022-05433-z>.
- [26] C. Felser, L. Wollmann, S. Chadov, G.H. Fecher, S.S.P. Parkin, Basics and perspective of magnetic Heusler compounds, *Apl. Mater.* 3 (4) (2015), <https://doi.org/10.1063/1.4917387>.
- [27] C.T. Tanaka, J. Nowak, J.S. Moodera, C.T. Tanaka, J. Nowak, J.S. Moodera, Spin-polarized tunneling in a half-metallic ferromagnet, *J. Appl. Phys.* 6239 (86) (1999) 9–13, <https://doi.org/10.1063/1.371678>.
- [28] C. Hordequin, J.P. Nozières, J. Pierre, Half metallic NiMnSb -based spin-valve structures, *J. Magn. Magn. Mater.* 183 (1–2) (1998) 225–231, [https://doi.org/10.1016/S0304-8853\(97\)01072-X](https://doi.org/10.1016/S0304-8853(97)01072-X).
- [29] H. Mehnane, B. Bekkouche, S. Kacimi, A. Hallouche, M. Djermouni, A. Zaoui, First-principles study of new half Heusler for optoelectronic applications, *Superlattice. Microst.* 51 (6) (2012) 772–784, <https://doi.org/10.1016/j.spmi.2012.03.020>.
- [30] S. Kacimi, H. Mehnane, A. Zaoui, I-II-V and I-III-IV half-Heusler compounds for optoelectronic applications: comparative ab initio study, *J. Alloys Compd.* 587 (2014) 451–458, <https://doi.org/10.1016/j.jallcom.2013.10.046>.
- [31] H.C. Kandpal, C. Felser, R. Seshadri, Covalent bonding and the nature of band gaps in some half-Heusler compounds, *J. Phys. Appl. Phys.* 39 (5) (2006) 776–785, <https://doi.org/10.1088/0022-3727/39/5/S02>.
- [32] F. Casper, T. Graf, S. Chadov, B. Balke, C. Felser, Half-Heusler compounds: novel materials for energy and spintronic applications, *Semicond. Sci. Technol.* 27 (6) (2012), <https://doi.org/10.1088/0268-1242/27/6/063001>.
- [33] A. Azouaoui, A. Hourmatallah, N. Benzakour, K. Bouslykhane, First-principles study of optoelectronic and thermoelectric properties of LiCaX ($X=\text{N, P and As}$) half-Heusler semiconductors, *J. Solid State Chem.* 310 (February) (2022) 123020, <https://doi.org/10.1016/j.jssc.2022.123020>.
- [34] V. Robert, H. Franz, Die ternETren Nitride LiMgN und LiZnN , *Zeitschrift fuer anorganische Chemie* 657 (August) (1948) 1–12.
- [35] H. Nowotny, K. Bachmayer, Die Verbindungen LiMgP , LiZnP und LiZnAs , *Monatsh. Chem.* 81 (4) (1950) 488–496, <https://doi.org/10.1007/BF00906437>.
- [36] S. Bounab, Y. Bouhadda, A. Bentabet, Theoretical prediction of the structural, elastic, electronic, and thermodynamic properties of the Nowotny-Juza LiMgAs Sb 1-x alloy, *Comput. Condens. Matter* 21 (2019) e00401, <https://doi.org/10.1016/j.cocom.2019.e00401>.
- [37] A. Amudhavalli, R. Rajeswarapalanichamy, K. Iyakutti, A.K. Kushwaha, First principles study of structural and optoelectronic properties of Li based half Heusler alloys, *Comput. Condens. Matter* 14 (November 2017) (2018) 55–66, <https://doi.org/10.1016/j.cocom.2018.01.002>.
- [38] H. Alam, S. Ramakrishna, A review on the enhancement of figure of merit from bulk to nano-thermoelectric materials, *Nano Energy* 2 (2) (2013) 190–212, <https://doi.org/10.1016/j.nanoen.2012.10.005>.
- [39] K. Berland, N. Shulumba, O. Hellman, C. Persson, O.M. Løvvik, Thermoelectric transport trends in group 4 half-Heusler alloys, *J. Appl. Phys.* 126 (14) (2019) 145102, <https://doi.org/10.1063/1.5117288>.
- [40] J.B. Gu, C.J. Wang, Y. Cheng, L. Zhang, L.C. Cai, G.F. Ji, Structural, elastic, thermodynamic, electronic properties and phase transition in half-Heusler alloy NiVsB at high pressures, *Comput. Mater. Sci.* 96 (PA) (2015) 72–80, <https://doi.org/10.1016/j.commatsci.2014.08.049>.
- [41] K. Kaur, R. Kumar, D.P. Rai, A promising thermoelectric response of HfRhSb half Heusler compound at high temperature : a first principle study, *J. Alloys Compd.* 763 (2018) 1018–1023, <https://doi.org/10.1016/j.jallcom.2018.06.034>.
- [42] N.S. Chauhan, S. Bathula, B. Gahtori, et al., Spinodal decomposition in $(\text{Ti, Zr})\text{CoSb}$ half-Heusler: a nanostructuring route toward high efficiency thermoelectric materials, *J. Appl. Phys.* 126 (12) (2019), <https://doi.org/10.1063/1.5109091>.
- [43] Y. Xia, S. Bhattacharya, V. Ponnambalam, A.L. Pope, S.J. Poon, T.M. Tritt, Thermoelectric properties of semimetallic $(\text{Zr, Hf})\text{CoSb}$ half-Heusler phases, *J. Appl. Phys.* 88 (4) (2000) 1952–1955, <https://doi.org/10.1063/1.1305829>.
- [44] G. Surucu, M. Isik, A. Candan, X. Wang, H.H. Gullu, Investigation of structural, electronic, magnetic and lattice dynamical properties for XCoBi (X: Ti, Zr, Hf) Half-Heusler compounds, *Phys. B Condens. Matter* 587 (February) (2020) 412146, <https://doi.org/10.1016/j.physb.2020.412146>.
- [45] R.J. Quinn, J.W.G. Bos, Advances in half-Heusler alloys for thermoelectric power generation, *Mater. Adv.* 2 (19) (2021) 6246–6266, <https://doi.org/10.1039/d1ma00707f>.
- [46] S.J. Poon, Recent advances in thermoelectric performance of half-heusler compounds, *Metals* 8 (12) (2018), <https://doi.org/10.3390/met8120989>.
- [47] F. Peng, H.Z. Fu, X.D. Yang, Transition phase and thermodynamic properties of PtC from first-principles calculations, *Solid State Commun.* 145 (3) (2008) 91–94, <https://doi.org/10.1016/j.jssc.2007.10.030>.
- [48] Z. Dong, J. Luo, C. Wang, et al., Half-Heusler-like compounds with wide continuous compositions and tunable p- to n-type semiconducting thermoelectrics, *Nat. Commun.* 13 (1) (2022) 1–9, <https://doi.org/10.1038/s41467-021-27795-3>.
- [49] T. Sekimoto, K. Kurosaki, H. Mutu, S. Yamanaka, Thermoelectric properties of $(\text{Ti, Zr, Hf})\text{CoSb}$ type half-heusler compounds, *Mater. Trans.* 46 (7) (2005) 1481–1484.
- [50] D. Zhao, M. Zuo, L. Bo, Y. Wang, Synthesis and thermoelectric properties of Pd-doped ZrCoBi half-heusler compounds, *Mater. Article* 11 (728) (2018) 1–9, <https://doi.org/10.3390/ma11050728>.
- [51] R. Gautier, X. Zhang, L. Hu, et al., Prediction and accelerated laboratory discovery of previously unknown 18-electron ABX compounds, *Nat. Chem.* 7 (April) (2015) 308–316, <https://doi.org/10.1038/nchem.2207>.

- [52] Y. Benallou, K. Amara, B. Doumi, M. Zemouli, B.B. Allel, O. Arbouche, Structural stability , electronic structure , and novel transport properties with high thermoelectric performances of ZrlrX (X = as , Bi , and Sb), *J. Comput. Electron.* 16 (1) (2017) 1–11, <https://doi.org/10.1007/s10825-016-0937-8>.
- [53] M. Yazdani-Kachoei, S. Jalali-Asadabadi, Topological analysis of electron density in half-Heusler ZrXBi (X ¼ Co , Rh) compounds : a density functional theory study accompanied by Bader ' s quantum theory of atoms in molecules, *J. Alloys Compd.* 828 (2020) 154287, <https://doi.org/10.1016/j.jallcom.2020.154287>.
- [54] S. Chibani, O. Arbouche, K. Amara, et al., A computational study of the optoelectronic and thermoelectric properties of HfIrX (X = As, Sb and Bi) in the cubic LiAlSi-type structure, *J. Comput. Electron.* 16 (3) (2017) 765–775, <https://doi.org/10.1007/s10825-017-1008-5>.
- [55] N. Arikian, G. DikiCi Yıldız, Y.G. Yıldız, A. İyigör, Electronic, elastic, vibrational and thermodynamic properties of HfIrX (X = as, Sb and Bi) compounds: insights from DFT-based computer simulation, *J. Electron. Mater.* 49 (5) (2020) 3052–3062, <https://doi.org/10.1007/s11664-020-08029-6>.
- [56] S. Chibani, O. Arbouche, M. Zemouli, et al., Ab initio prediction of the structural, electronic, elastic, and thermoelectric properties of half-heusler ternary compounds TiIrZ (X = as and Sb), *J. Electron. Mater.* 47 (1) (2018) 196–204, <https://doi.org/10.1007/s11664-017-5761-9>.
- [57] I.K. Durukan, Y.O. Ciftci, ANALYSIS OF CoTiSb COMPOUND BY FIRST PRINCIPLES METHOD, in: 4. Uluslararası Mühendislik Bilimleri Ve Multidisipliner Yaklaşımlar Kongresi, 2022, pp. 302–307. <http://www.muhendisbilimlerkongresi.org/>.
- [58] K. Burke, Perspective on density functional theory, *Phys. J Chem.* 136 (2012) 150901, <https://doi.org/10.1063/1.4704546>.
- [59] I.B. Obot, D.D. Macdonald, Z.M. Gasem, Density functional theory (DFT) as a powerful tool for designing new organic corrosion inhibitors . Part 1 : an overview, *Corrosion Sci.* 99 (2015) 1–30, <https://doi.org/10.1016/j.corsci.2015.01.037>.
- [60] Maylis Orio, A. Panzatis Dimitrios, F. Neese, Density functional theory, 2009, *Photosynth. Res.* 102 (2009) 443–453, <https://doi.org/10.1007/s11120-009-9404-8>.
- [61] N. Mahmood, R. Ahmad, G. Murtaza, Ab initio investigations of structural, elastic, mechanical, electronic, magnetic, and optical properties of half-heusler compounds RhCrZ (Z = Si, Ge), *J. Supercond. Nov. Magnetism* 30 (9) (2017) 2481–2488, <https://doi.org/10.1007/s10948-017-4051-3>.
- [62] G. Kresse, J. Hafner, Ab initio molecular dynamics for liquid metals, *Phys. Rev. B* 47 (1) (1993) 558–561, <https://doi.org/10.1103/PhysRevB.47.558>.
- [63] I.K. Durukan, Y.O. Ciftci, First-principles study on B2 based XAl (X = Rh , Ru) compounds, *Phys. Scripta* 96 (2021) 125726, <https://doi.org/10.1088/1402-4896/ac3b6d>.
- [64] G. Kresse, J. Hafner, Ab initio molecular-dynamics simulation of the liquid-metamorphous- semiconductor transition in germanium, *Phys. Rev. B* 49 (20) (1994) 14251–14269, <https://doi.org/10.1103/PhysRevB.49.14251>.
- [65] G. Kresse, J. Furthmüller, Efficiency of ab-initio total energy calculations for metals and semiconductors using a plane-wave basis set, *Comput. Mater. Sci.* 6 (1) (1996) 15–50, [https://doi.org/10.1016/0927-0256\(96\)00008-0](https://doi.org/10.1016/0927-0256(96)00008-0).
- [66] J.P. Perdew, K. Burke, M. Ernzerhof, Generalized gradient approximation made simple, *Phys. Rev. Lett.* 77 (18) (1996) 3865–3868, <https://doi.org/10.1103/PhysRevLett.77.3865>.
- [67] Hendrik J. Monkhorst, James D. Pack, Special points for Brillouin-zone integrations, *Phys. Rev. B* 13 (12) (1976) 5188, <https://doi.org/10.1103/PhysRevB.13.5188>.
- [68] Y.O. Ciftci, M. Evecen, First principle study of structural, electronic, mechanical, dynamic and optical properties of half-Heusler compound LiScSi under pressure, *Phase Transitions* 91 (12) (2018) 1206–1222, <https://doi.org/10.1080/01411594.2018.1515433>.
- [69] Z. Ran, C. Zou, Z. Wei, H. Wang, VELAS : an open-source toolbox for visualization and analysis of elastic anisotropy, *Comput. Phys. Commun.* 283 (2023) 108540, <https://doi.org/10.1016/j.cpc.2022.108540>.
- [70] A. Togo, F. Oba, I. Tanaka, First-principles calculations of the ferroelastic transition between rutile-type and CaCl₂-type SiO₂ at high pressures, *Phys. Rev. B Condens. Matter* 78 (13) (2008) 1–9, <https://doi.org/10.1103/PhysRevB.78.134106>.
- [71] F. Peng, H. Fu, X. Yang, Ab initio study of phase transition and thermodynamic properties of PtN, *Phys. B Condens. Matter* 403 (17) (2008) 2851–2855, <https://doi.org/10.1016/j.physb.2008.02.022>.
- [72] F. Peng, H.Z. Fu, X.L. Cheng, First-principles calculations of thermodynamic properties of TiB₂ at high pressure, *Phys. B Condens. Matter* 400 (1–2) (2007) 83–87, <https://doi.org/10.1016/j.physb.2007.06.020>.
- [73] Sadeghi M, Zelati A, Boochani A, Arman A, Mirzaei S. Thermoelectric Behavior of the CrTiZ (Z = as , P) Half-Heuslers : a DFT Study Comparing Half-Metallic , MOKE , and Thermoelectric Behavior of the CrTiZ (Z FOAO = FOAO as , P) Half-Heuslers : a DFT Study.
- [74] F.D. Murnaghan, Physics: f. d. murnaghan. *PROC N A S* 30 (1944) 244–247.
- [75] M. Javed, M.A. Sattar, M. Benkraouda, N. Amrane, Structural and mechanical stability , lattice dynamics and electronic structure of the novel CrVZ (Z = S , Se , & Te) half-Heusler alloys, *Mater. Today Commun.* 25 (2020) 101519, <https://doi.org/10.1016/j.mtcomm.2020.101519>.
- [76] Y. Zhang, X. Xu, Machine learning modeling of lattice constants for half-Heusler alloys Machine learning modeling of lattice constants for half-Heusler alloys, *AIP Adv.* 10 (2020) 045121, <https://doi.org/10.1063/5.0002448>.
- [77] I.K. Durukan, Y.O. Ciftci, First-principles calculations of vibrational and optical properties of half- Heusler NaScSi, *Indian J. Phys.* 95 (11) (2021) 2303–2312, <https://doi.org/10.1007/s12648-020-01887-0>.
- [78] C. Xie, H. Yuan, Z. Zhang, X. Wang, Magnetic Weyl and quadratic nodal lines in inverse-Heusler-based fully compensated ferrimagnetic half-metals, *Phys. Rev. Mater.* 6 (9) (2022) 1–8, <https://doi.org/10.1103/PhysRevMaterials.6.094406>.
- [79] B. Balke, K. Kroth, G.H. Fecher, C. Felser, A New Diluted Magnetic Semiconductor: the Half-Metallic Ferromagnet CoTi_{1-x}FexSb, 2018.
- [80] R. Murugeswari, A.M.F. Benjal, R. Rajeswarapalanichamy, DFT studies on structural stability and magnetic properties of XTiSb (X = Fe , Co) DFT studies on structural stability and magnetic properties of XTiSb (X = Fe , Co), in: INNational Conference on Current Advancements in Physics 3rd&4th February 2017, 2019, <https://doi.org/10.9790/4861-17002023437>, 37–37.
- [81] K. Ravikumar, K. Kiran, V.S. Sreebalaji, Characterization of mechanical properties of aluminium/tungsten carbide composites, *Measurement* 102 (2017) 142–149, <https://doi.org/10.1016/j.measurement.2017.01.045>.
- [82] J.N. Coleman, U. Khan, W.J. Blau, Y.K. Gun, Small but strong : a review of the mechanical properties of carbon nanotube – polymer composites 44 (2006) 1624–1652, <https://doi.org/10.1016/j.carbon.2006.02.038>.
- [83] K. Wang, M.K. Mishra, C.C. Sun, Exceptionally Elastic Single-Component Pharmaceutical Crystals, 2019, pp. 5–10, <https://doi.org/10.1021/acs.chemmater.9b00040>. Published online.
- [84] M. Meier, E. John, D. Wieckhusen, W. Wirth, W. Peukert, In fl uence of mechanical properties on impact fracture : prediction of the milling behaviour of pharmaceutical powders by nanoindentation, *Powder Technol.* 188 (3) (2009) 301–313, <https://doi.org/10.1016/j.powtec.2008.05.009>.
- [85] R. Mauludin, D. Mudhakir, D. Umeha, S.N. Soewandhi, O.D. Putra, E. Yonemochi, Crystal formation 111 (September 2017) (2018) 65–72, <https://doi.org/10.1016/j.jeps.2017.09.035>.
- [86] L. Wang, C. Wang, S. Wu, Y. Fan, X. Li, *Biomaterials Science*, 2020, pp. 2714–2733, <https://doi.org/10.1039/d0bm00269k>. Published online.
- [87] S. Mitragotri, J. Lahann, Physical approaches to biomaterial design 8 (JANUARY) (2009) 15–23, <https://doi.org/10.1038/nmat2344>.
- [88] S. Lv, D.M. Dudek, Y. Cao, M.M. Balamurali, J. Gosline, H. Li, Designed biomaterials to mimic the mechanical properties of muscles, *Nature* 465 (May) (2010), <https://doi.org/10.1038/nature09024>.
- [89] H. Gu, L. Bumke, C. Chluba, E. Quandt, R.D. James, Phase engineering and supercompatibility of shape memory alloys, *Mater. Today* 21 (3) (2018) 265–277, <https://doi.org/10.1016/j.matto.2017.10.002>.
- [90] Shen G, Wang L, Chen D, Shen G. Materials for flexible electronics. doi:10.1039/c7cs00278e.
- [91] Y. Hu, L. You, B. Xu, et al., Ferroelastic-switching-driven large shear strain and piezoelectricity in a hybrid ferroelectric, *Nat. Mater.* 20 (May) (2021), <https://doi.org/10.1038/s41563-020-00875-3>.
- [92] S.H. Baek, H.W. Jang, C.M. Folkman, et al., Ferroelastic switching for nanoscale non-volatile magnetoelectric devices 9 (April) (2010) 309–314, <https://doi.org/10.1038/nmat2703>.
- [93] T. Seki, C. Feng, K. Kashiyama, S. Sakamoto, Y. Takasaki, Photoluminescent ferroelastic molecular crystals 8628 (2020) 8924–8928, <https://doi.org/10.1002/ange.201914610>.
- [94] M De Jong, W. Chen, T. Angsten, et al., Charting the Complete Elastic Properties of Inorganic Crystalline Compounds, 2015, pp. 1–13, <https://doi.org/10.1038/sdata.2015.9>. Published online.
- [95] D.G. Cahill, S.K. Watson, R.O. Pohl, D.R. Clarke, G.J. Snyder, E.S. Toberer, Lower limit to the thermal conductivity of disordered crystals, *Phys. Rev. B* 46 (10) (1992) 6131–6140, <https://doi.org/10.1103/PhysRevB.46.6131>.
- [96] D.R. Clarke, C.G. Levi, Materials design for the next generation thermal barrier coatings, *Annu. Rev. Mater. Res.* 33 (July) (2003) 383–417, <https://doi.org/10.1146/annurev.matsci.33.011403.113718>.
- [97] O.L. Anderson, C. Liedermann, Relevant to Geophysics since several comprehensive reviews exist [e . g ., Hearmon 6 (4) (1968) 491–524.
- [98] B.B. Karki, L. Stixrude, R.M. Wentzcovitch, High-pressure elastic properties of major of earth ' S from first principles, 2001, pp. 507–534.
- [99] F. Mouhat, F.X. Couder, Necessary and sufficient elastic stability conditions in various crystal systems, *Phys. Rev. B Condens. Matter* 90 (22) (2014) 4–7, <https://doi.org/10.1103/PhysRevB.90.224104>.
- [100] M.H. Elahmar, H. Rached, D. Rached, et al., Structural, mechanical, electronic and magnetic properties of a new series of quaternary Heusler alloys CoFeMnZ (Z=Si, As, Sb): a first-principle study, *J. Magn. Magn. Mater.* 393 (2015) 165–174, <https://doi.org/10.1016/j.jmmm.2015.05.019>.
- [101] L. Zhang, X. Wang, Z. Cheng, Electronic, magnetic, mechanical, half-metallic and highly dispersive zero-gap half-metallic properties of rare-earth-element-based quaternary Heusler compounds, *J. Alloys Compd.* 718 (2017) 63–74, <https://doi.org/10.1016/j.jallcom.2017.05.116>.
- [102] M. Benkabou, H. Rached, A. Abdellaoui, et al., Electronic structure and magnetic properties of quaternary Heusler alloys CoRhMnZ (Z = Al, Ga, Ge and Si) via first-principle calculations, *J. Alloys Compd.* 647 (2015) 276–286, <https://doi.org/10.1016/j.jallcom.2015.05.273>.
- [103] S. Liu, Y. Zhan, J. Wu, X. Chen, H. Ye, Site preference of the alloying additions on mechanical and electronic properties of B2 ZrRu-based compounds, *Comput. Mater. Sci.* 117 (2016) 1–6, <https://doi.org/10.1016/j.commatsci.2016.01.019>.
- [104] X.Q. Chen, H. Niu, D. Li, Y. Li, Modeling hardness of polycrystalline materials and bulk metallic glasses, *Intermetallics* 19 (9) (2011) 1275–1281, <https://doi.org/10.1016/j.intermet.2011.03.026>.
- [105] T.M. Bhat, D.C. Gupta, Transport, structural and mechanical properties of quaternary FeVTiAl alloy, *J. Electron. Mater.* 45 (11) (2016) 6012–6018, <https://doi.org/10.1007/s11664-016-4827-4>.

- [106] D. Chen, Z. Chen, J. Cai, Z. Chen, Preparation of W-Al intermetallic compound powders by a mechanochemical approach, *J. Alloys Compd.* 461 (1–2) (2008), <https://doi.org/10.1016/j.jallcom.2007.07.058>.
- [107] D. Jiang, M. Wu, D. Liu, F. Li, M. Chai, S. Liu, Structural stability, electronic structures, mechanical properties and debye temperature of transition metal impurities in tungsten: a first-principles study, *Metals* 9 (9) (2019), <https://doi.org/10.3390/met9090967>.
- [108] M.K. Bangbose, P.O. Adebambo, G.T. Solola, G.A. Adebayo, Exploring the electronic fitness function, effective mass, elastic and transport properties of Rh₁P Half-Heusler alloy, *Mater. Sci. Eng. B: Solid-State Mater. Adv. Technol.* 264 (March 2020) (2021), <https://doi.org/10.1016/j.mseb.2020.114987>.
- [109] R. Ahmad, N. Mehmood, Investigation of half-heusler compounds RhCrZ ($Z = P$, as, Sb, Sn): a first principle study, *J. Supercond. Nov. Magnetism* 31 (8) (2018) 2637–2645, <https://doi.org/10.1007/s10948-017-4472-z>.
- [110] I. Muhammad, J.M. Zhang, A. Ali, M.U. Rehman, S. Muhammad, Structural, mechanical, thermal, magnetic, and electronic properties of the RhMnSb half-Heusler alloy under pressure, *Mater. Chem. Phys.* 251 (March) (2020) 123110, <https://doi.org/10.1016/j.matchemphys.2020.123110>.
- [111] M. Ibrir, S. Lakel, S. Berri, S. Alleg, R. Bensalem, Ab initio study of structural, electronic, magnetic alloys: XTiSb ($X = Co$, Ni and Fe), *AIP Conf. Proc.* 1653 (April) (2015), <https://doi.org/10.1063/1.4914237>.
- [112] D. Joubert, From ultrasoft pseudopotentials to the projector augmented-wave method, *Phys. Rev. B Condens. Matter* 59 (3) (1999) 1758–1775, <https://doi.org/10.1103/PhysRevB.59.1758>.
- [113] X. Zeng, R. Peng, Y. Yu, Z. Hu, Y. Wen, L. Song, Pressure effect on elastic constants and related properties of Ti3Al intermetallic compound: a first-principles study, *Materials* 11 (10) (2018), <https://doi.org/10.3390/ma11102015>.
- [114] S. Ganeshan, S.L. Shang, H. Zhang, Y. Wang, M. Mantina, Z.K. Liu, Elastic constants of binary Mg compounds from first-principles calculations, *Intermetallics* 17 (5) (2009) 313–318, <https://doi.org/10.1016/j.intermet.2008.11.005>.
- [115] L. Vitos, P.A. Korzhavyi, B. Johansson, Stainless steel optimization from quantum mechanical calculations, *Nat. Mater.* 2 (1) (2003) 25–28, <https://doi.org/10.1038/nmat790>.
- [116] H. Ledbetter, A. Migliori, H. Ledbetter, A. Migliori, A general elastic-anisotropy measure A general elastic-anisotropy measure 63516 (2006) 1–6, <https://doi.org/10.1063/1.2338835>.
- [117] P. Prelovšek, Temperature and doping dependence of the high-energy Kink in Cuprates 36402 (January) (2008) 1–4, <https://doi.org/10.1103/PhysRevLett.100.036402>.
- [118] V. Tvergaard, J.W. Hutchinson, Microcracking in ceramics induced by thermal expansion or elastic anisotropy 66 (16) (1988) 157–166.
- [119] A. Schmitz, Elastic anisotropy a N D the substitutional 37 (12) (1989) 3151–3155.
- [120] C.M. Rost, E. Sachet, T. Borman, et al., Entropy-stabilized oxides, *Nat. Commun.* (2015), <https://doi.org/10.1038/ncomms9485>. Published online.
- [121] Pitike KC, Marquez-rossy AE, Flores-betancourt A, et al. On the Elastic Anisotropy of the Entropy-Stabilized Oxide (Mg, Co, Ni, Cu, Zn)O Compound. doi:10.1063/5.0011352.
- [122] H. Olijnyk, A.P. Jephcoat, Optical zone-centre phonon modes and macroscopic elasticity in hcp metals 115 (2000) 335–339.
- [123] P.S.M.J. Spoer, Physical review letters 6 75 (19) (1995) 3462–3465.
- [124] S.I. Ranganathan, M. Ostoya-starzewski, Universal elastic anisotropy index, *Phys. Rev. Lett.* 101 (55504) (2008) 3–6, <https://doi.org/10.1103/PhysRevLett.101.055504>.
- [125] C.M. Kube, Elastic anisotropy of crystals, *AIP Adv.* 6 (2016) 095209, <https://doi.org/10.1063/1.4962996>.
- [126] A.N.A. Simoes, A quantum chemical dialogue mediated by textbooks : pauling 's "the nature of the chemical bond" and coulson 's "valence", author (s): ana simões source : notes and records of the royal society of London , Vol. 1, 62 , No . 3 (Sep . 20 , 2008), Notes Rec R Soc 62 (3) (2014) 259–269, <https://doi.org/10.1098/rsnr.2007.0005>.
- [127] J.A. Duffy, Ultraviolet transparency of glass : a chemical approach in terms of band theory , polarisability and electronegativity, *Phys. Chem. Glasses* 42 (3) (2001) 151–157.
- [128] A.S. Verma, solidi 199 (1) (2009) 192–199, <https://doi.org/10.1002/pssb.200844242>.
- [129] M. Zeeshan, H.K. Singh, J. Van Den Brink, H.C. Kandpal, Ab initio design of new cobalt-based half-Heusler materials for thermoelectric applications, *Phys. Rev. Mater.* 1 (7) (2017) 1–9, <https://doi.org/10.1103/PhysRevMaterials.1.075407>.
- [130] J. Wang, H. Yuan, Y. Liu, X. Wang, G. Zhang, Multiple dimensions of spin-gapless semiconducting states in tetragonal Sr₂CuF₆, *Phys. Rev. B* 106 (6) (2022) 1–6, <https://doi.org/10.1103/PhysRevB.106.L060407>.
- [131] G. Ding, J. Wang, Z.M. Yu, Z. Zhang, W. Wang, X. Wang, Single pair of type-III Weyl points half-metals: BaNiO₆ as an example, *Phys. Rev. Mater.* 7 (1) (2023) 14202, <https://doi.org/10.1103/PhysRevMaterials.7.014202>.
- [132] Y. Yang, C. Xie, Y. Cui, X. Wang, W. Wu, Maximally charged single-pair multi-Weyl point phonons in P23 -type BeH₂, *Phys. Rev. B* 107 (5) (2023) 1–7, <https://doi.org/10.1103/PhysRevB.107.054310>.
- [133] G. Ding, T. Sun, X. Wang, Ideal nodal-net, nodal-chain, and nodal-cage phonons in some realistic materials, *Phys. Chem. Chem. Phys.* (2022) 11175–11182, <https://doi.org/10.1039/d2cp00731b>. Published online.
- [134] C. Xie, Y. Liu, Z. Zhang, et al., Sixfold degenerate nodal-point phonons: symmetry analysis and materials realization, *Phys. Rev. B* 104 (4) (2021) 1–8, <https://doi.org/10.1103/PhysRevB.104.045148>.
- [135] H. Shang, C. Carbogno, P. Rinke, M. Scheffler, Lattice dynamics calculations based on density-functional perturbation theory in real space, *Comput. Phys. Commun.* 215 (2017) 26–46, <https://doi.org/10.1016/j.cpc.2017.02.001>.
- [136] M. Moradi, N. Taheri, M. Rostami, Structural, electronic, magnetic and vibrational properties of half-Heusler NaZrZ ($Z = P$, As, Sb) compounds, *Phys. Lett., Section A: Gen. Atom. Solid State Phys.* 382 (41) (2018) 3004–3011, <https://doi.org/10.1016/j.physleta.2018.07.008>.
- [137] G. Lan, B. Ouyang, J. Song, The role of low-lying optical phonons in lattice thermal conductance of rare-earth pyrochlores: a first-principle study, *Acta Mater.* 91 (2015) 304–317, <https://doi.org/10.1016/j.actamat.2015.03.004>.
- [138] E.K. Dogan, S.E. Gulebaglan, Some properties of LiInSi half-Heusler alloy via density functional theory, *Bull. Mater. Sci.* 44 (3) (2021) 1–7, <https://doi.org/10.1007/s12034-021-02499-y>.
- [139] A. Candan, S. Akbudak, M. Özdurán, A. İyigör, An examination of the structural, electronic, elastic, vibrational and thermodynamic properties of Ru2YGa ($Y = Sc$, Ti and V) Heusler alloys, *Chin. J. Phys.* 56 (4) (2018) 1772–1780, <https://doi.org/10.1016/j.cjph.2018.05.006>.
- [140] V. Kumar, J.N. Lakshmi, R. Jain, A. Rani, Electronic structure , elastic , magnetic , and optical properties of Fe 2 MnZ ($Z = Si$, Ge , and Sn) full heusler alloys : first-principle calculations v (2019) 739–749.
- [141] J.K. Bairwa, M. Rani, P.K. Kamlesh, et al., Modeling and simulation of multifaceted properties of X2NaIO₆ ($X = Ca$ and Sr) double perovskite oxides for advanced technological applications, *J. Mol. Model.* 29 (12) (2023) 1–13, <https://doi.org/10.1007/s00894-023-05786-z>.
- [142] U. Rani, P.K. Kamlesh, R. Singh, et al., Exploring properties of organometallic double perovskite (CH 3 NH 3) 2 AgInCl 6 : a novel material for energy conversion devices 2450144 (2024) 1–15, <https://doi.org/10.1142/S0217984924501446>.
- [143] P.K. Kamlesh, R. Gautam, S. Kumari, A.S. Verma, Investigation of inherent properties of XScZ ($X = Li$, Na, K; $Z = C$, Si, Ge) half-Heusler compounds: appropriate for photovoltaic and thermoelectric applications, *Phys. B Condens. Matter* 615 (August 2020) (2021) 412536, <https://doi.org/10.1016/j.physb.2020.412536>.
- [144] S. Yalameha, A. Vaez, Ab-initio thermodynamic and elastic properties of AlNi and AlNi₃ intermetallic compounds, *Int. J. Mod. Phys. B* 32 (11) (2018), <https://doi.org/10.1142/S0217979218501291>.
- [145] H. Joshi, D.P. Rai, L. Hnamte, A. Laref, R.K. Thapa, A theoretical analysis of elastic and optical properties of half Heusler MoCoSb ($M=Ti$, Zr and Hf), *Heliyon* 5 (3) (2019) e01155, <https://doi.org/10.1016/j.heliyon.2019.e01155>.
- [146] S. Zahir, N. Mehmood, R. Ahmad, S. Khan, A.U. Rahman, A. Dahshan, Structural, elastic, mechanical, electronic, magnetic and optical properties of half-Heusler compounds CoFeZ ($Z = P$, As, Sb): a GGA+U approximation, *Mater. Sci. Semicond. Process.* 143 (June 2021) (2022) 106445, <https://doi.org/10.1016/j.mssp.2021.106445>.
- [147] J. Sun, H. Wang, Ab Initio Investigations of Optical Properties of the High-Pressure Phases of ZnO, 2005, pp. 1–5, <https://doi.org/10.1103/PhysRevB.71.125132>. Published online.
- [148] B. Anissa, D. Radouan, B. Benaouda, Optical and thermoelectric response of RhTiSb half-Heusler, *Int. J. Mod. Phys. B* 33 (22) (2019) 1–12, <https://doi.org/10.1142/S0217979219502473>.
- [149] M. Kumari, U.P. Verma, Full potential study of HoMg, *J. Magnesium Alloys* 6 (2) (2018) 189–196, <https://doi.org/10.1016/j.jma.2018.03.002>.
- [150] P. Mondal, S. Khanom, N.A. Shahed, M.K. Hossain, F. Ahmed, An ab initio insight into the structural, physical, thermodynamic and optoelectronic properties of superconducting Heusler-like LiGa₂Rh, *Phys. C: Supercond. Appl.* 603 (August) (2022) 1354142, <https://doi.org/10.1016/j.physc.2022.1354142>.
- [151] O. Douinat, A. Boucherdou, A. Seghier, et al., Theoretical investigation of the physical, mechanical, and thermal properties of Zr₂XB₁Ni₂ ($X: Al$, Ga) double half-Heusler alloys, *J. Mater. Res.* 38 (20) (2023) 4509–4521, <https://doi.org/10.1557/s43578-023-01165-9>.
- [152] M. Naseri, D.M. Hoat, First principles investigation on elastic, optoelectronic and thermoelectric properties of KYX ($X = Ge$, Sn and Pb) half-heusler compounds, *J. Mol. Graph. Model.* 92 (2019) 249–255, <https://doi.org/10.1016/j.jmgm.2019.08.002>.
- [153] R. Meenakshi, R.A.S. Srinivasan, A. Amudhavalli, K. Iyakutti, Electronic Structure , Magnetic , Optical and Transport Properties of Half-Heusler Alloys RhFeZ ($Z = P$, as , Sb , Sn , Si , Ge , Ga , in , Al) – A DFT Study, 2021, <https://doi.org/10.1080/01411594.2021.1944626>. Published online.
- [154] A.O. Alrashdi, A. Asif, M.M. Fadhlani, A. Bakar, A. Afaq, J. Alqahtani, First principles calculations to investigate electronic, magnetic anisotropy energy and optical properties of MnCrP half-Heusler alloy, *J. Mater. Res. Technol.* 20 (2022) 4220–4230, <https://doi.org/10.1016/j.jmrt.2022.08.149>.
- [155] N. Mehmood, R. Ahmad, Structural, electronic, magnetic, and optical properties of half-heusler alloys RuMnZ ($Z = P$, as): a first-principle study, *J. Supercond. Nov. Magnetism* 31 (1) (2018) 233–239, <https://doi.org/10.1007/s10948-017-4196-0>.
- [156] F. Mostari, A. Rahman, R. Khatun, First principles study on the structural, elastic, electronic and optical properties of cubic 'half-heusler' alloy RuVAS under pressure, *Int. J. Mater. Math. Sci.* 2 (4) (2020) 51–63, <https://doi.org/10.34104/ijmms.020.051063>.
- [157] F. Benzoudji, O.M. Abid, T. Seddik, et al., Insight into the structural, elastic, electronic, thermoelectric, thermodynamic and optical properties of MRhSb ($M = Ti$, Zr, Hf) half-Heuslers from ab initio calculations, *Chin. J. Phys.* 59 (October 2018) (2019) 434–448, <https://doi.org/10.1016/j.cjph.2019.04.009>.
- [158] M.A. Blanco, E. Francisco, V. Luña, GIBBS: isothermal-isobaric thermodynamics of solids from energy curves using a quasi-harmonic Debye model, *Comput. Phys.*

- Commun. 158 (1) (2004) 57–72, <https://doi.org/10.1016/j.comphy.2003.12.001>.
- [159] M. Sarwan, V.A. Shukoor, M.F. Shareef, S. Singh, A first principle study of structural, elastic, electronic and thermodynamic properties of Half-Heusler compounds; YNiPn (Pn=As, sb, and bi), Solid State Sci. 112 (November 2020) (2021) 106507, <https://doi.org/10.1016/j.solidstatosciences.2020.106507>.
- [160] M.A. Bennani, Z. Aziz, Structural , electronic , magnetic , elastic , thermodynamic , and thermoelectric properties of the half-heusler RhFeX (with X = Ge , Sn) compounds, Publ. Online (2021) 211–225.
- [161] D. Kalita, M. Ram, N. Limbu, R. Kalita, A. Saxena, Prediction of some physical properties in new half Heusler alloy NbAgSi, J. Solid State Chem. 310 (February) (2022) 122999, <https://doi.org/10.1016/j.jssc.2022.122999>.
- [162] Y. Sefir, S. Terkhi, Z. Zitouni, et al., Structural, electronic, magnetic and thermodynamic properties of the new multifunctional half-Heusler alloy CoTeSn: half-metallic and ferromagnetic behaviour, Pramana - J. Phys. 95 (2) (2021), <https://doi.org/10.1007/s12043-021-02125-w>.
- [163] B. Anissa, D. Radouan, B. Benaouda, A. Omar, First-principles study of structural, electronic, thermodynamic, and thermoelectric properties of a new ternary half-Heusler alloy PdZrGe, Chin. J. Phys. 56 (6) (2018) 2926–2936, <https://doi.org/10.1016/j.cjph.2018.09.027>.
- [164] Chien-Min Sung, M. Sung, B. Anissa, D. Radouan, et al., Structural and electronic properties of WC, Chin. J. Phys. 56 (14) (1996) 2926–2936, <https://doi.org/10.1103/PhysRevB.38.9483>.
- [165] O. Sahnoun, H. Bouhani-Benziane, M. Sahnoun, M. Driz, C. Daul, Ab initio study of structural, electronic and thermodynamic properties of tungstate double perovskites Ba₂MW₆ (M = Mg, Ni, Zn), Comput. Mater. Sci. 77 (April 2018) (2013) 316–321, <https://doi.org/10.1016/j.commatsci.2013.04.053>.
- [166] M.S. Hossain, M.M. Hossain, Structural, mechanical, thermodynamic, electronic and optical characteristics of LaPtBi half-Heusler compound from first principles analyses, Ferroelectrics 585 (1) (2021) 118–127, <https://doi.org/10.1080/00150193.2021.1991210>.
- [167] D. Kalita, N. Limbu, M. Ram, A. Saxena, DFT study of structural, mechanical, thermodynamic, electronic, and thermoelectric properties of new PdT₁Z (Z = Ge and Pb) half Heusler compounds, Int. J. Quant. Chem. 122 (17) (2022) 1–13, <https://doi.org/10.1002/qua.26951>.
- [168] I.K. Durukan, Y.O. Ciftci, Ab-initio study on physical properties of intermetallic LiPb compound, J. Comput. Sci. 54 (May) (2021) 101428, <https://doi.org/10.1016/j.jocs.2021.101428>.
- [169] A. Touia, M. Benkhaled, C. Khobzaoui, M. Fodil, Optical and thermodynamic properties of half-heusler compound TaIrSn: using modified becke-Johnson (mBJ), J. Supercond. Nov. Magnetism 34 (11) (2021) 2865–2877, <https://doi.org/10.1007/s10948-021-05981-0>.